

1 **This manuscript has been published in EARTH AND PLANETARY SCIENCE LETTERS.**

2 <https://doi.org/10.1016/j.epsl.2025.119491>
3

4 **Constraints from uranium and molybdenum isotope ratios on the origin of enriched mid-**
5 **ocean ridge basalts**

6
7 Joel B. Rodney^{a*}, Morten B. Andersen^b, Bramley J. Murton^c, Tim Elliott^a
8

9 ^aBristol Isotope Group, School of Earth Sciences, University of Bristol, Wills Memorial Building,
10 Queen's Road, Bristol, BS8 1RJ, UK

11 ^bSchool of Earth & Environmental Sciences, Cardiff University, Park Place, Cardiff, CF10 3AT,
12 UK

13 ^cNational Oceanography Centre, Waterfront Campus, European Way, Southampton, SO14 3ZH,
14 UK

15 *Corresponding author

16 *Email addresses:* joel.rodney@bristol.ac.uk (J.B. Rodney), andersenm1@cardiff.ac.uk (M.B.
17 Andersen), bramley.murton@noc.ac.uk (B.J. Murton), tim.elliott@bristol.ac.uk (T. Elliott).
18
19
20
21
22
23

Abstract

Most mid-ocean ridge basalts (MORB) are depleted in highly incompatible elements relative to the primitive mantle and are termed normal (N)-MORB. Some MORB, erupted at ridge segments distal from mantle hot-spots, are enriched in incompatible elements. The origin of these enriched (E)-MORB is debated, although many studies have proposed that recycled oceanic crust shapes their compositions. Uranium (U) and molybdenum (Mo) isotope ratios have been argued to trace the contribution of recycled oceanic crust in the source of N-MORB, which has high $\delta^{238}\text{U}$ and low $\delta^{98/95}\text{Mo}$ relative to the bulk silicate Earth (BSE). Here, we provide U and Mo isotopic data on E-MORB samples from the northern mid-Atlantic ridge (13° & 45° N). We analysed hand-picked, leached MORB glass, yielding $^{234}\text{U}/^{238}\text{U}$ near secular equilibrium, therefore reflecting samples unperturbed by surface processes. Samples have uniform $\delta^{238}\text{U}$ and $\delta^{98/95}\text{Mo}$, with means of -0.307 ± 0.032 ‰, 2sd, and -0.14 ± 0.04 ‰, 2sd, respectively, both within uncertainty of BSE, and distinct from N-MORB. These data, as well as unremarkable Ce/Pb and radiogenic Pb isotopic compositions in E-MORB globally, are incompatible with their sources containing recycled oceanic crust or continental derived sediments. Instead, our data fit with a model of low degree partial melting of the uppermost mantle that metasomatises the sub-oceanic lithosphere. Given BSE-like U isotopic compositions of E-MORB, that are isotopically unfractionated during low degree partial melting, we suggest that the initial melting event must have occurred prior to the recycling of isotopically distinct in U oceanic crust into the upper mantle (i.e., prior to ca. 600 Ma, the estimated time of deep ocean oxygenation). Metasomatised portions of oceanic lithospheric mantle preserve these $\geq 600\text{Ma}$ U isotopic compositions, which are subducted and stirred back into the convecting upper mantle, ultimately to be sampled at ridges as E-MORB. Molybdenum

isotopic compositions of E-MORB are in line with such a model but also reflect isotopic fractionation to higher $\delta^{98/95}\text{Mo}$ during low degree partial melting of ≥ 600 Ma upper mantle, that counter acts the lowering of $\delta^{98/95}\text{Mo}$ in the upper mantle by an on-going process of plate recycling.

Keywords: U isotopes; Mo isotopes; Enriched MORB; Crustal recycling; low degree partial melting

1. Introduction

Mid-ocean ridge basalts (MORB), magmatic samples of the upper mantle, are chemically heterogeneous and commonly split into two groups according to their ‘incompatible’ element compositions (Fig. 1) (e.g., Schilling, 1975; Gale et al., 2013). Along the majority of mid-ocean ridge (MOR) segments, basalts erupted have ‘depleted’ signatures, with ratios of more to less incompatible elements lower than estimates of the primitive mantle (e.g., La/Sm normalized to primitive mantle, $(\text{La/Sm})_N < 1$) (Fig. 1) (McDonough and Sun, 1995). Rarer, enriched (E)-MORB have incompatible element abundances markedly higher than N-MORB and are associated with elevated ratios of more to less incompatible elements (e.g., $(\text{La/Sm})_N \geq 1$) and distinctive isotopic signatures (e.g., radiogenic $^{87}\text{Sr}/^{86}\text{Sr}$). While their presence is well documented, the exact definition of E-MORB varies in different studies (Fig. 1).

Some E-MORB locations are from topographically elevated MOR sections and are linked to enrichments from hot-spots, upwellings from greater depth (Schilling, 1975; Schilling et al., 1985). However, for E-MORB that occur at MOR segments far from the influence of hot-spots, the origin of the chemical enrichment is debated. It has been proposed that recycling of oceanic crust and/or continental sediments into the upper mantle causes enrichment (e.g., Allègre and Turcotte, 1986; Prinzhofer et al., 1989; Hémond et al., 2006; Waters et al., 2011; Ulrich et al., 2012; Yang et al., 2020), similar to models of source enrichment in ocean island basalts (OIB). Other works argue for low degree partial melting and two stage melting models, either with or without recycled crustal material. Donnelly et al. (2004) argue for low degree partial melting of subducting crust that enriches the convecting mantle wedge at subduction zones. This enriched mantle is stirred into the

wider upper mantle and can be sampled at ridges giving rise to E-MORB. Nielsen et al., (2018) propose a similar model but also argue for the addition of subducted sediment to the overlying mantle that induces low degree partial melting to produce the E-MORB reservoir that is ultimately sampled under ridges. Scenarios that do not invoke recycled crustal material in the E-MORB source argue for low degree partial melts of the uppermost mantle that metasomatise oceanic mantle lithosphere, enriching portions of mantle that are subsequently subducted back into the upper mantle and sampled at ridges (e.g., Green, 1971; Kostopoulos and Murton, 1992; Halliday et al., 1995; Niu et al., 2002; Chen et al., 2022; Guo et al., 2023).

Measurements of novel stable isotope ratios can be used to investigate upper mantle chemical heterogeneity and enrichment. Uranium (U) and molybdenum (Mo) are useful for tracing processes of crustal recycling due to large low temperature isotopic fractionations that occur during seafloor alteration of the oceanic crust, sediment deposition (Andersen et al., 2015; Freymuth et al., 2015; Ahmad et al., 2021), and during the dehydration of subducting slabs in subduction zones (Andersen et al., 2015; Freymuth et al., 2015, 2019; König et al., 2016; Gaschnig et al., 2017; Villalobos-Orchard et al., 2020; Ahmad et al., 2021). Here we express Mo isotope ratios as $\delta^{98/95}\text{Mo}_{\text{NIST SRM3134}}$ (the relative difference in $^{98}\text{Mo}/^{95}\text{Mo}$ between samples and standard reference material NIST SRM3134, hereafter written $\delta^{98/95}\text{Mo}$ in the text), and U isotope ratios as $\delta^{238}\text{U}_{\text{CRM145}}$ (the relative difference in $^{238}\text{U}/^{235}\text{U}$ between samples and certified reference material CRM-145, hereafter written $\delta^{238}\text{U}$ in the text).

Slab dehydration during subduction releases oxidising fluids with high $\delta^{98/95}\text{Mo}$ and low $\delta^{238}\text{U}$ into the overlying mantle wedge, as inferred from the compositions of volcanic arc lavas (Andersen et

al., 2015; Freymuth et al., 2015, 2019; König et al., 2016; Gaschnig et al., 2017; Villalobos-Orchard et al., 2020) (Fig. 2). Exhumed eclogites and metasediments with low $\delta^{98/95}\text{Mo}$ also reflect this process (Fig. 2a) (Chen et al., 2019; Ahmad et al., 2021). Additionally, in some cases mafic oceanic crust has acquired a low $\delta^{98/95}\text{Mo}$ through seafloor alteration before subduction zone processing (Ahmad et al., 2021). The U isotopic system further reflects the importance of seawater alteration of the oceanic crust (Fig. 2b). Seawater alteration of oceanic crust strongly increases its U concentration (e.g., Staudigel et al., 1995) with the added U, on average, being isotopically heavy (Andersen et al., 2015, 2024). Subducting slab dehydration and seawater alteration therefore result in residual slabs with compositions that are isotopically light in Mo and isotopically heavy in U. The recycling of Mo and U from this crustal material into the upper mantle is inferred from compositions of N-MORB samples that are isotopically lighter in Mo and heavier in U than the bulk silicate Earth (BSE) as defined by chondrites (Burkhardt et al., 2014; Andersen et al., 2015; Hin et al., 2022) (Fig. 2). This can also be seen in higher Ce/Mo ratios and lower Th/U ratios of N-MORB than the BSE. Cerium and Th are of similar incompatibility to Mo and U respectively during mantle melting, but with different fluid mobility; Mo and U are aqueous fluid mobile, Ce and Th are not.

Following the onset of the first major rise in atmospheric oxygen (~ 2.3 Ga), there would have been a supply of continental derived U to the oceans due to oxidative weathering. The recycling of oceanic crust with excess U relative to immobile Th has been used to explain the lower measured $^{232}\text{Th}/^{238}\text{U}$ in MORB relative to the time integrated $^{232}\text{Th}/^{238}\text{U}$ ratio calculated from Pb isotopic compositions (e.g., Zartman and Haines, 1988; McCulloch, 1993; Collerson and Kamber, 1999; Elliott et al., 1999). Isotopically perturbed U, however, may only have been recycled into the

mantle since the Neoproterozoic oxygenation event, ~ 600 Ma (e.g., Lyons et al., 2014), given that imparting high $\delta^{238}\text{U}$ to altered oceanic crust (AOC) requires oxygenated deep oceans (Andersen et al., 2015, 2024). Isotopically perturbed Mo, in contrast, has potentially been recycled into the N-MORB source since the onset of modern day like plate tectonics and mass balance models suggest that at least ~ 1 Gyr of crustal recycling is needed to cause the observed shift in N-MORB $\delta^{98/95}\text{Mo}$ from BSE compositions (Hin et al., 2022).

Molybdenum and U isotopes offer a way to investigate if recycled oceanic crust is mixed into the E-MORB source and provide constraints on the timescales it takes to ‘pollute’ the upper mantle with surface derived material. Recent studies have shown some E-MORB have chondritic or slightly higher values of $\delta^{98/95}\text{Mo}$ and are resolvable from N-MORB (Bezard et al., 2016; Chen et al., 2022). To assess if this is a ubiquitous feature, there is need for data from different geographic regions, as well as for measurements of both $\delta^{98/95}\text{Mo}$ and $\delta^{238}\text{U}$ on the same samples. Herein we combine Mo with U isotopic measurements on a set of E-MORB samples from the northern Mid-Atlantic ridge (MAR) as a diagnostic test for recycled crustal components in the E-MORB source.

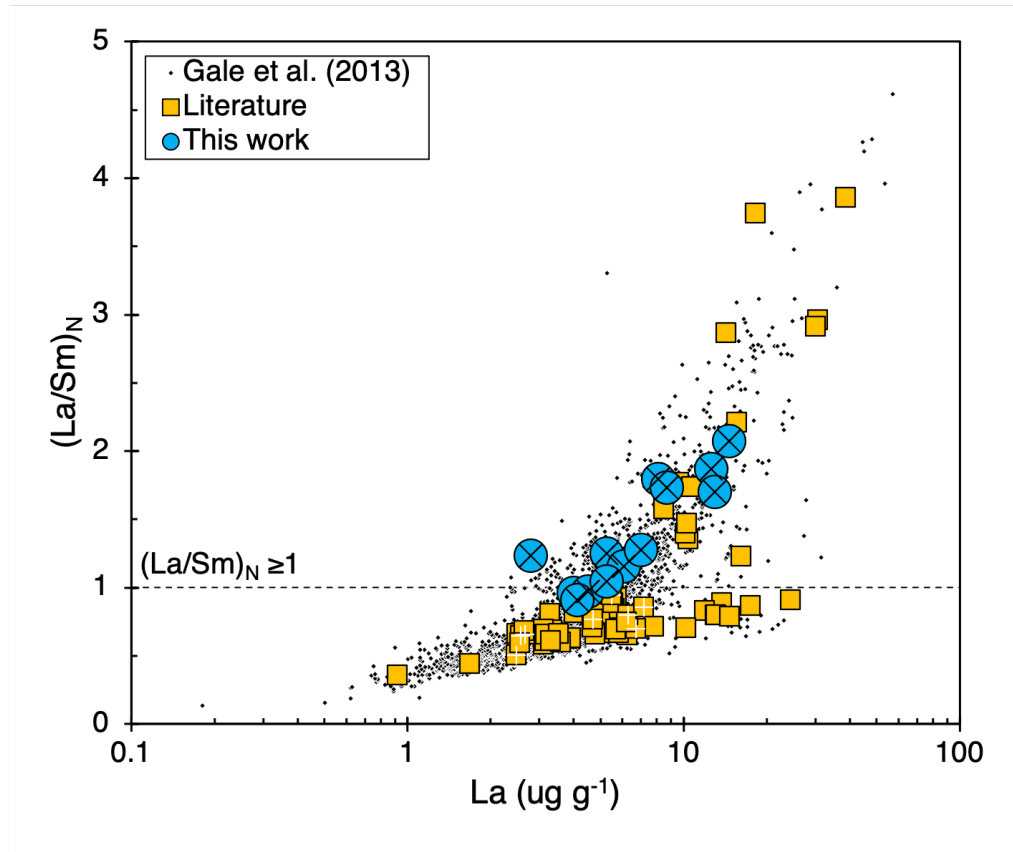


Fig. 1. Global MORB variations in chemical enrichment based on $(La/Sm)_N$. Mid-ocean ridge basalts database from Gale et al. (2013) shown as small black diamonds. Literature MORB data with Mo and/or U isotopic data are shown as yellow squares (Andersen et al., 2015; Bezard et al., 2016; Chen et al., 2022; Hin et al., 2022). Mid-ocean ridge basalt samples analysed in this study are shown as larger blue circles. Samples in this work and literature data with both Mo and U isotope data are shown with black crosses (E-MORB) or white plus signs (N-MORB).

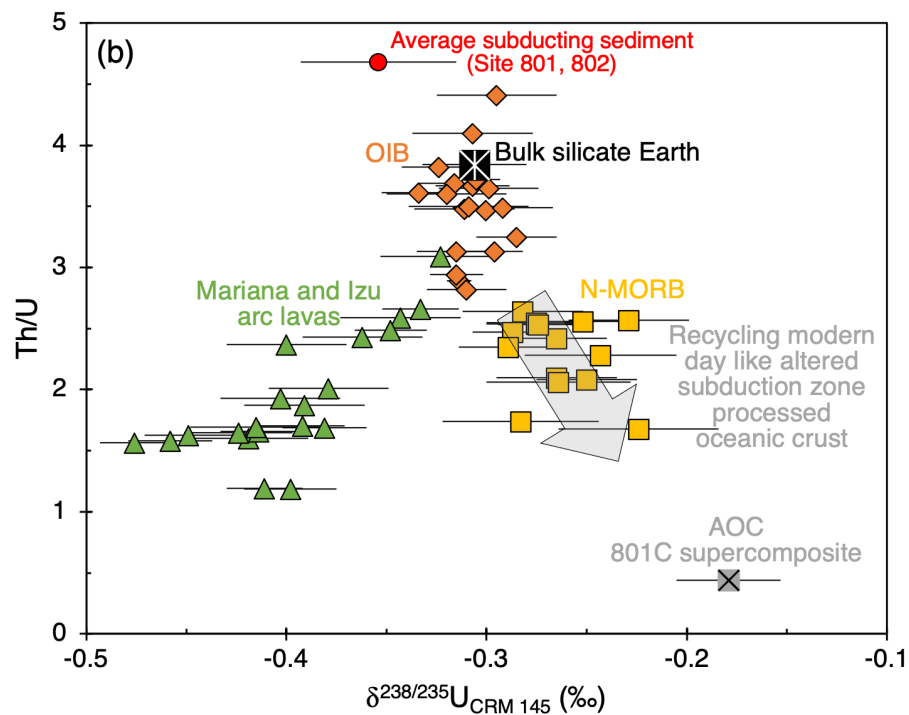
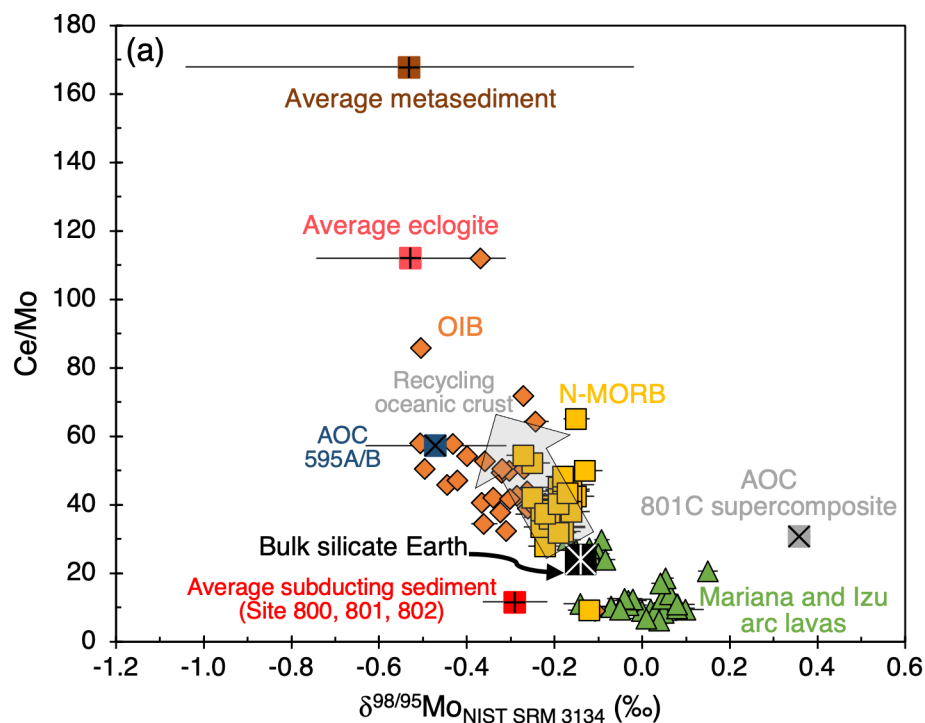


Fig. 2. (a) $\delta^{98/95}\text{Mo}$ versus Ce/Mo and (b) $\delta^{238}\text{U}$ versus Th/U for mantle derived basalts, AOC, subduction processed N-MORB-like eclogite and subducting sediment. Ocean island basalts (orange diamonds) are from Willbold and Elliott (2023) and Andersen et al. (2015). Volcanic arc lavas from the Mariana and Izu arc (green triangles) are from Freymuth et al. (2015, 2019), Andersen et al. (2015), and Vilalobos-Orchard et al. (2020). Bulk silicate Earth compositions (black starred square) are from Hin et al. (2022) and Andersen et al. (2015). Average Western Pacific subducting sediment composition (red square with a plus sign) is from Ocean Drilling Programme sites 800, 801, and 802 from Andersen et al. (2015) and Freymuth et al. (2015). We use the global average subducting sediment Th/U ratio from Plank (2014) GLOSS-II. Average compositions of AOC from the 801C supercomposite (grey crossed square) are from Andersen et al. (2015) and Freymuth et al. (2015). Average AOC from 595A/B (blue crossed square) is the average composition, $\pm 1\text{sd}$, weighted by Mo concentration from Ahmad et al. (2021). Average composition, $\pm 1\text{sd}$, weighted by Mo concentration of a set of exhumed eclogites (pink square with a plus sign) are from Chen et al. (2019) and Ahmad et al. (2021). Average composition, $\pm 1\text{sd}$, weighted by Mo concentration of metasediments (brown square with a plus sign) is from Ahmad et al. (2021). Mid-ocean ridge basalt data (yellow squares) are from Andersen et al. (2015), Bezard et al. (2016), Chen et al. (2022), and Hin et al. (2022). For MORB Mo data we follow the filtering of Hin et al. (2022), where two anomalous samples from Bezard et al. (2016) are excluded, as they do so themselves. We also exclude all data from Liang et al. (2017), whose data cannot be reproduced and show markedly higher $\delta^{98/95}\text{Mo}$ compositions for MORB samples than Bezard et al. (2016) and Chen et al. (2022), see Hin et al. (2022) for details. Grey arrows show the effect of mixing recycled oceanic crust into the mantle.

2. Geological location and samples

We report U and Mo elemental and isotopic compositions for sixteen MAR E-MORB samples, located at $\sim 13^\circ \text{ N } 44^\circ \text{ W}$ (five samples) and $45^\circ \text{ N } 28^\circ \text{ W}$ (eleven samples) that span MgO contents from ~ 10 to 7 wt. %. Our samples are chemically enriched, with either $(\text{La}/\text{Sm})_{\text{N}} \geq 1$ and or $\text{K}_2\text{O}/\text{TiO}_2 \geq 0.11$. Enriched-MORB in the $13^\circ \text{ N } 44^\circ \text{ W}$ segment are common, and basalts have up to forty times higher concentrations of highly incompatible elements than N-MORB from segments nearby (Bougault et al., 1988). Samples from $13^\circ \text{ N } 44^\circ \text{ W}$ were collected by dredging in the RSS James Cook JC007 cruise in March – April 2007 (Wilson et al., 2013) (Table S1). They represent a group of basalts erupted before the formation of oceanic core complexes in the area, and now sit off-axis, having been erupted at $\sim 0.5 - 1$ Ma. Samples from $\sim 45^\circ \text{ N } 28^\circ \text{ W}$ are also from a region where E-MORB commonly occurs (Bougault et al., 1988) and samples were collected *in situ* during RSS James Cook cruise JC024 May – June 2008 and are all < 3 Ma (Table S1) (Searle et al., 2010). Major and trace element data for both sample sets were collected following the methods in Wilson et al. (2013).

The Azores hot-spot at $\sim 38^\circ \text{ N } 28^\circ \text{ W}$, which forms the Azores Island chain sitting to the east of the MAR, is the closest mantle hot-spot to both sample sites. The Azores hot-spot interacts with the MAR, causing nearby ridge segments to become broader and shallower. Material from the Azores hot-spot flows southwards along the ridge, with elevated La/Sm ratios between 35° to 40° N . More N-MORB like compositions occur below 30° N and above 40° N , with no detectable effects of the hot-spot further south than 26° N (e.g., Maia et al., 2007). Our sample sites sit outside

the zone of influence of the Azores hot-spot, and geochemical enrichment is not linked to hot-spot-
ridge interaction (Bougault et al., 1988).

3. Methods

Fresh MORB glass was crushed and processed to $\sim 600 \mu\text{m}$ size chips, using an agate pestle and mortar. To avoid samples potentially affected by seawater alteration (e.g., Fe-Mn oxide coatings), samples were hand-picked under a binocular microscope to ensure samples were optically clear and devoid of potential alteration. While this process has long been employed, notably in U-series disequilibrium studies (e.g., Reinitz and Turekian, 1989), it is laborious, and considering the quantities needed for isotopic analysis (e.g., $>1 \text{ g}$), it is a rate limiting step. Hand picking MORB glass is also subjective, and it is unclear what defines an acceptable limit of quality. A reliable check of sample alteration in young samples is given by measurements of $^{234}\text{U}/^{238}\text{U}$ activity ratios. If unaffected by recent seawater alteration, the ^{238}U decay chain will be in secular equilibrium, and so the activity ratio of $^{234}\text{U}/^{238}\text{U}$, typically expressed as $(^{234}\text{U}/^{238}\text{U})$, will be unity. Seawater has $(^{234}\text{U}/^{238}\text{U}) \sim 1.14$ (e.g., Kipp et al., 2022) and elevated $(^{234}\text{U}/^{238}\text{U})$ in samples may indicate the addition of seawater U and other elements onto Fe-Mn oxide coatings (Siebert et al., 2003; Hin et al., 2022). We explored varyingly stringent picking strategies on samples. Up to three different splits of glass of varying quality (A, B, and C in decreasing order of quality) were prepared (classifications are detailed in Supplementary Material: Section 1) (Fig. S1). In some cases, different splits were combined to ensure there was enough sample to measure.

Samples also underwent a reductive leaching step (Supplementary Material: Section 1) prior to dissolution to remove secondary coatings. Samples were leached with a mixture of 0.05 M hydroxylamine hydrochloride, 15 % acetic acid and 0.03 M Na-EDTA buffered to pH 4 with NaOH (Gutjahr et al., 2007). Andersen et al. (2015) and Hin et al (2022) note that leaching can result in

some glass dissolution, and minor U and Mo loss (Fig. S2). Ratios of the concentrations of elements that absorb to Fe-Mn coatings such as U and Mo to those little affected, such as Th, that would only be removed during glass dissolution, were monitored to examine the effects of leaching. Samples of JC24-82-21 were prepared and analysed before other samples to calibrate methods. This sample was leached three times and results indicated that one to two leaching steps were sufficient to remove any apparent chemical signature of Fe-Mn coatings (Fig. S3). For other samples we opted for two leaching steps, although note that one step is likely sufficient.

Uranium isotopic measurement methods followed Andersen et al. (2015), and Mo isotopic measurement methods followed Willbold et al. (2016) and Hin et al. (2022), as detailed fully in Supplementary Material: Section 2. Uranium and Mo isotope analyses were conducted in the Bristol Isotope Group labs, University of Bristol. Approximately 0.5 to 1 g of MORB glass was dissolved and after achieving full dissolution, a $\sim 1\%$ fraction of samples was measured on an Element2 ICP-MS for Th, U, and Mo concentration (Andersen et al., 2014). Measured reference materials are in good agreement with literature values (Supplementary Material: Section 2) (Table S2).

Samples were spiked with the IRMM3636 $^{236}\text{U} - ^{233}\text{U}$ 50:50 double spike (Richter et al., 2008) aiming for a $^{236}\text{U}/^{235}\text{U}$ ratio of 5. Samples were also spiked with an in-house $^{97}\text{Mo} - ^{100}\text{Mo}$ double spike, with a $^{97}\text{Mo}/^{95}\text{Mo}$ ratio of 47.58 and $^{100}\text{Mo}/^{95}\text{Mo}$ ratio of 58.32, aiming for a natural Mo-double spike Mo proportion of 0.5.

Purification and U separation used a two-column method, with TRU resin to separate most matrix elements, including all Mo, followed by UTEVA resin to separate Th from U. An aliquot containing Mo from the first separation column was collected for later processing. Final U aliquots were dissolved in 0.2 M HCl (aiming for U concentration of 100 – 300 ng g⁻¹) for isotopic analysis. Procedural blanks were <30 pg U, negligible compared to amount of U consumed per measurement, 30 – 80 ng.

Uranium isotope compositions were measured on a ThermoFinnigan Neptune MC-ICP-MS (serial no. 1002) in low mass resolution ($M/\Delta M \sim 2000$, 5 to 95 % peak height definition). Samples were introduced into the plasma using a $\sim 40 \text{ ul min}^{-1}$ micro-concentric PFA nebuliser connected to a Cetac Aridus (1st generation) desolvating system. Masses 232 (²³²Th), 233 (²³³U), 234 (²³⁴U), 235 (²³⁵U), 236 (²³⁶U), and 238 (²³⁸U) were measured simultaneously. Each sample was preceded and followed by a measurement of the double-spiked CRM-145 standard. Individual measurements consisted of 80 cycles, with 4.194 s integration time.

Uranium isotope ratios for ²³⁸U/²³⁵U and ²³⁴U/²³⁸U were calculated using the exponential mass fractionation law and double spike ²³³U/²³⁶U ratio (Richter et al., 2008). Data reported are normalised to the average of the bracketing CRM-145 standard, with ²³⁴U/²³⁸U ratios reported in delta notation relative to secular equilibrium where secular equilibrium is 0 and CRM-145 has a $\delta^{234}\text{U}$ value of -38.6 ‰ (Cheng et al., 2013).

External reproducibility of all samples has been determined from the long-term external reproducibility of BHVO-2 measured at various intensities (Supplementary Material: Section 2).

This results in an estimated external reproducibility of $\delta^{238}\text{U}$ and $\delta^{234}\text{U}$ from ± 0.09 to 0.03 ‰ ,
2sd, and ± 4 to 0.9 ‰ , 2sd, for ^{238}U intensities from 200 – 1000 pA ranges respectively (Fig. S4).
Uranium isotopic measurements of international reference materials (BHVO-2, BCR-2, BIR, W-
2A, and CZ-1) agree with literature values (Table S3).

Collected Mo fractions from the TRU resin U chemistry were dried and dissolved for Mo
chemistry using Eichrom AG 1-X8 anionic resin. Final Mo collections were dried and re-dissolved
in 0.4 M HNO_3 – 0.4 M HF for a Mo concentration of 200 ng g^{-1} for isotopic analysis. Procedural
blanks were $<400\text{ pg Mo}$, negligible compared to the amount of Mo consumed per measurement,
 $\sim 30\text{ ng}$.

Molybdenum isotope compositions were measured on a ThermoFinnigan Neptune MC-ICP-MS
(serial no. 1020) in low mass resolution ($M/\Delta M \sim 1600$, 5 to 95 % peak height definition). Samples
were introduced to the plasma using a $\sim 40\text{ ul min}^{-1}$ micro-concentric PFA nebuliser connected to
a Cetac Aridus (1st generation) desolvating system. Masses 91 (^{91}Zr), 92 (^{92}Mo), 95 (^{95}Mo), 96
(^{96}Mo), 97 (^{97}Mo), 98 (^{98}Mo), 99 (^{99}Ru), 100 (^{100}Mo), and 101 (^{101}Ru) were measured
simultaneously. Each sample was preceded and followed by a measurement of the double-spiked
standard NIST SRM3134. Individual measurements consisted of 30 cycles, with 4.194 s
integration time.

Measurements were internally normalised with a double spike inversion using the isotopes ^{95}Mo ,
 ^{97}Mo , ^{98}Mo , and ^{100}Mo . Samples were then externally normalised to the spiked bracketing standard
NIST SRM3134 to calculate $\delta^{98/95}\text{Mo}$. Data were corrected for ^{98}Ru and ^{100}Ru interferences using

both ^{99}Ru and ^{101}Ru respectively as monitors of Ru intensity; both corrections yielded the same Mo isotope ratios within uncertainty of one another and uncorrected data. We take a homoscedastic approach to determine our external reproducibility, pooled 2sd, on any single stable Mo isotopic measurement (i.e., one standard-sample-standard measurement) (Table S4). Using this approach, we define an external reproducibility of $\delta^{98/95}\text{Mo} \pm 0.05 \text{ ‰}$, 2sd, for a single measurement in a given run. This pooled 2sd is then used to calculate the standard error for a given sample given the number, n , of repeat measurements, typically 4 to 6 for unknown samples. This is identical to the 2sd, $\pm 0.05 \text{ ‰}$, of 35 repeats of W-2A measured over 4 digestions across 4 measuring sessions, and is similar to that reported in Chen et al. (2022) and Hin et al. (2022). Molybdenum isotopic measurements of international reference materials (BHVO-2, BCR-2, and W-2A) agree with literature data (Table S5).

4. Results

Our MAR samples have chemical enrichments from $(\text{La}/\text{Sm})_{\text{N}}$ 0.91 to 2.07 ($\text{K}_2\text{O}/\text{TiO}_2$ 0.11 to 0.37) (Fig. 1, table S6). Uranium concentrations range from 101 to 443 ng g^{-1} , all enriched relative to average N-MORB (83 ng g^{-1} , Gale et al., 2013) (Table S6). Molybdenum concentrations range from 189 to 967 ng g^{-1} , which is above and below average N-MORB (360 ng g^{-1} , Gale et al., 2013) (Table S6). There are positive correlations between U and Mo concentrations with $(\text{La}/\text{Sm})_{\text{N}}$ (Fig. 3a, b).

Values of $\delta^{238}\text{U}$ show little variation between $-0.331 \pm 0.019 \text{‰}$, 2se, and $-0.263 \pm 0.028 \text{‰}$, 2se, with a concentration weighted average of $-0.307 \pm 0.032 \text{‰}$, 2sd, (Fig. 3c, table S6). The variability is similar to our long-term external reproducibility of samples measured at similar conditions $\sim \pm 0.03 \text{‰}$ and reflects a near uniform composition of our sample set. The $\delta^{238}\text{U}$ compositions of the different qualities of glass picked and leached are all, bar one sample, within analytical uncertainty (Fig. S5a). Also, samples bar JC-24-89-13, are within uncertainty of secular equilibrium (Fig. S5b). Sample JC-24-89-13, which is only +2.5 ‰ in $\delta^{234}\text{U}$ (Fig. S5b), also has a similar $\delta^{238}\text{U}$ to other samples (Fig. S5a). Our E-MORB $\delta^{238}\text{U}$ average is lower than global N-MORB, which has a concentration weighted average of $-0.259 \pm 0.041 \text{‰}$, 2sd, (Andersen et al., 2015) (Fig. 3c). We also report $\delta^{238}\text{U}$ data for four N-MORB samples from the Indian ocean basin (04/13C, 05/15G, 08/26F, 12/37F) additional to the N-MORB samples in Andersen et al. (2015), but reported in Hin et al. (2022) for $^{234}\text{U}/^{238}\text{U}$ data. These data are provided in the supplementary material and were collected following methods in Andersen et al. (2015). Our E-MORB $\delta^{238}\text{U}$ average is indistinguishable from BSE, $\delta^{238}\text{U} -0.306 \pm 0.026 \text{‰}$, 2se, (Andersen et al., 2015).

412

413 Molybdenum isotopic compositions show little variation with $\delta^{98/95}\text{Mo}$ ranging between $-0.11 \pm$
414 0.01 ‰ , 2se, and $-0.19 \pm 0.02 \text{ ‰}$, 2se, and are within analytical uncertainty of a concentration
415 weighted average of $-0.14 \pm 0.04 \text{ ‰}$, 2sd, (Fig. 3d, table S6). The variability, $\pm 0.04 \text{ ‰}$, 2sd, is
416 smaller than our long-term external reproducibility and reflects the near uniform composition of
417 our sample set. Our E-MORB concentration weighted average $\delta^{98/95}\text{Mo}$ is indistinguishable from
418 the value reported in Hin et al., (2022) for global E-MORB, $-0.12 \pm 0.03 \text{ ‰}$, 95 % c.i. The $\delta^{98/95}\text{Mo}$
419 compositions of the different qualities of glass picked and leached are all within analytical
420 uncertainty (Fig. S5c). Our E-MORB $\delta^{98/95}\text{Mo}$ average is higher than global N-MORB, $\delta^{98/95}\text{Mo}$
421 $-0.19 \pm 0.01 \text{ ‰}$, 95 % c.i. and indistinguishable from BSE, $\delta^{98/95}\text{Mo} -0.14 \pm 0.02 \text{ ‰}$, 95 % c.i.
422 (Fig. 3d) (Hin et al., 2022).

423

424 There are no correlations of $\delta^{238}\text{U}$ and $\delta^{98/95}\text{Mo}$ in our E-MORB samples with tracers of chemical
425 enrichment (Fig. 3c, d). There are no correlations between U and Mo isotopic compositions and
426 indicators of magmatic differentiation (Fig. S6). Samples from 13° N and 45° N show no
427 resolvable differences and we find no reason to treat each site differently. In summary, the
428 concentration weighted averages of $\delta^{238}\text{U}$ and $\delta^{98/95}\text{Mo}$ for our E-MORB samples is distinct from
429 global N-MORB, but indistinguishable from BSE (Fig. 3c, d) (Andersen et al., 2015; Hin et al.,
430 2022).

431

432

433

434

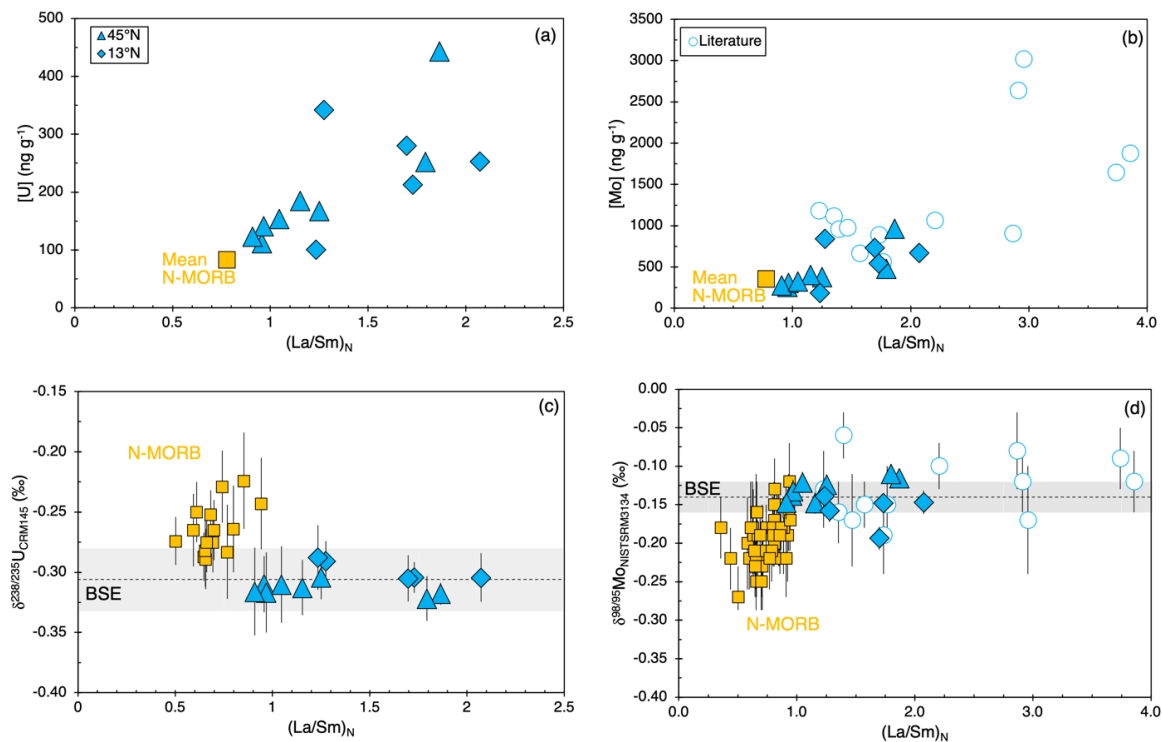


Fig. 3. (a) U and (b) Mo concentrations and (c) $\delta^{238}U$ and (d) $\delta^{98/95}Mo$ versus $(La/Sm)_N$ of MORB samples. Enriched-MORB from this study are shown as filled blue symbols and grouped into samples from 45°N (triangles) and 13°N (diamonds) and shown with $\pm 2se$ uncertainties. Average N-MORB (yellow squares) concentrations are from Gale et al. (2013). Isotopic data for BSE and N-MORB are from the same sources as in figure 2, and literature E-MORB (hollow circles) are from Bezard et al. (2016), Chen et al. (2022) and Hin et al. (2022). Grey shaded regions represents isotopic compositions of BSE ($\pm 2se$).

5. Discussion

5.1 Potential alteration of U and Mo isotopes

The reductive leaching process removed some U but little Mo, reflecting the presence of minimal secondary mineral hosted Mo (Supplementary Material: Section 1) (Fig. S2). The different qualities of picked glass for each sample measured showed similar patterns in leaching and are all largely within uncertainty in $\delta^{238}\text{U}$, $\delta^{98/95}\text{Mo}$, and $\delta^{234}\text{U}$ (all near secular equilibrium) (Fig. S3, S5). We therefore average all different splits measured for samples into overall $\delta^{238}\text{U}$, $\delta^{98/95}\text{Mo}$, and $\delta^{234}\text{U}$ compositions for each sample (Supplementary material: section 1). We further test that our hand-picked MORB glass samples reflect primary magmatic compositions by examining mixing relationships between our average E-MORB compositions and predicted compositions of Fe-Mn crusts. Iron-Mn crusts acquire U from seawater, with elevated $\delta^{234}\text{U}$, and have low $\delta^{238}\text{U}$ and $\delta^{98/95}\text{Mo}$, $\sim -0.69\text{‰}$ and -0.92‰ respectively (Siebert et al., 2003; Goto et al., 2014). In a binary mixing calculation between our average E-MORB composition and Fe-Mn crusts in $\delta^{238}\text{U}$ - $\delta^{234}\text{U}$ and $\delta^{98/95}\text{Mo}$ - $\delta^{234}\text{U}$ space, our samples do not form arrays towards the composition of Fe-Mn crusts (Fig. 4). The minor variability in $\delta^{238}\text{U}$ and $\delta^{98/95}\text{Mo}$ appears unrelated to $\delta^{234}\text{U}$, and the samples with minor deviations in $\delta^{234}\text{U}$ from secular equilibrium do not show compositions systematically perturbed towards Fe-Mn crusts in either U or Mo isotopic compositions (Fig. 4). We therefore infer that the $\delta^{238}\text{U}$ and $\delta^{98/95}\text{Mo}$ of the samples represent primary values.

5.2 Fractional crystallisation

Our data span a narrow range of MgO content (10.2 to 6.9 wt. %) and show no correlation in $\delta^{98/95}\text{Mo}$ and $\delta^{238}\text{U}$ with magmatic differentiation (Fig. S6). This is in accordance with other studies that show no resolvable correlation of $\delta^{98/95}\text{Mo}$ in MORB with MgO over a wider range of compositions, 1.8 to 9.5 wt.% (Bezard et al., 2016; Chen et al., 2022). Our samples also reflect the similar incompatibilities of U & Th and Mo & Ce during magmatic differentiation (Fig. S6), with near constant ratios of ~ 3 and ~ 35 respectively, in keeping with wider data for seafloor basalts (e.g., Gale et al., 2013).

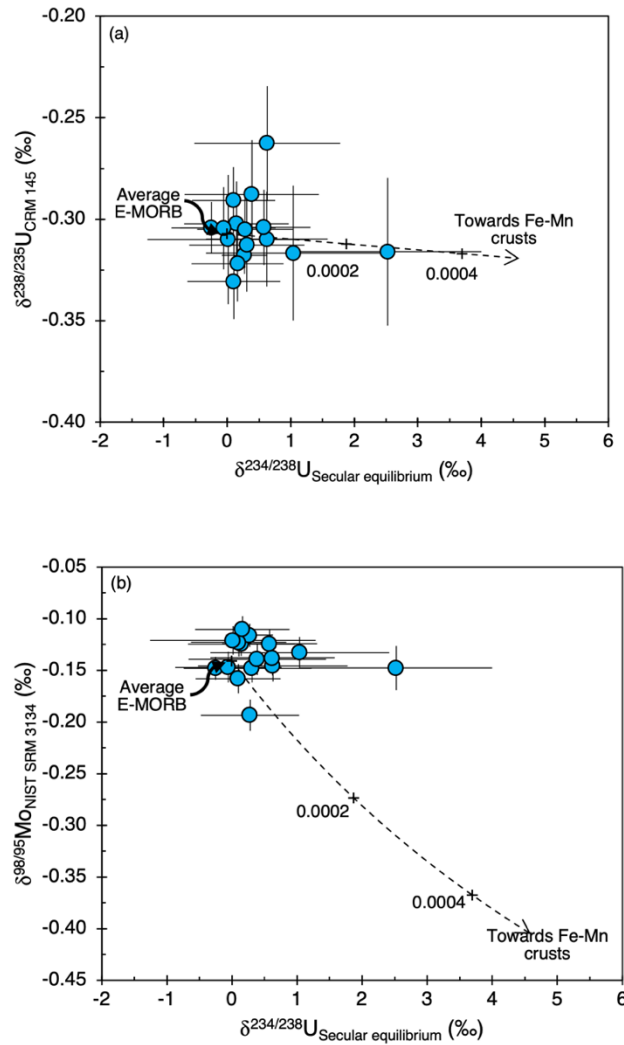


Fig. 4. Modelled mixing curves of $\delta^{234}\text{U}$ versus (a) $\delta^{238}\text{U}$ and (b) $\delta^{98/95}\text{Mo}$, showing the trajectory of Fe-Mn crust addition to our average E-MORB composition (dashed line). Values along the mixing curves show the mass fraction of Fe-Mn crust in the mixture. Compositions used in the mixing calculation are, E-MORB, $\delta^{238}\text{U} = -0.307\text{‰}$, $\delta^{234}\text{U} = 0\text{‰}$, $[\text{U}] = 202\text{ ng g}^{-1}$, $\delta^{98/95}\text{Mo} = -0.14\text{‰}$, and $[\text{Mo}] = 465\text{ ng g}^{-1}$. Fe-Mn crust, $\delta^{238}\text{U} = -0.69\text{‰}$, $\delta^{234}\text{U} = 146.3\text{‰}$, $[\text{U}] = 13100\text{ ng g}^{-1}$, $\delta^{98/95}\text{Mo} = -0.92\text{‰}$, and $[\text{Mo}] = 477000\text{ ng g}^{-1}$ (Henderson and Burton, 1999; Siebert et al., 2003; Goto et al., 2014).

5.3 Recycled crustal material in the E-MORB source

Recent work from Yang et al. (2020) suggests, based on compatible element abundances, that E-MORB geochemistry is explained by the mixture of low degree partial melts of garnet-clinopyroxene pyroxenite (i.e., recycled oceanic crust), with depleted MORB like melts. Melting of this recycled material and mixing with depleted MORB melts generates distinct compositions of element ratios, such as lower Ge/Si, in E-MORB relative to depleted MORB (Yang et al., 2020). The dehydration of subducting slabs during subduction zone processing strips oceanic crust of fluid mobile elements, resulting in high fluid mobile/fluid immobile element ratios in arc lavas. Complementary compositions should then be seen in E-MORB if they contain recycled crustal components, but E-MORB are enriched in both fluid mobile and immobile elements, and have no depletions in elements such as Nb, Tb, and Ti as seen in arc lavas (Niu et al., 2002, their figure 9). To reproduce some of the such E-MORB characteristics in their mixing models, Yang et al. (2020) suggest the recycling of upper continental crust material, that is enriched in elements such as Rb, Ba, and Pb, along with recycled oceanic crust to explain high Rb/Sr, Ba/La, and low Zr/Pb ratios of E-MORB.

Subducted sediments, a proxy for upper continental crust material, are distinctly enriched in Pb and have low Ce/Pb ratios and high $^{207}\text{Pb}/^{204}\text{Pb}$ ratios relative to $^{206}\text{Pb}/^{204}\text{Pb}$ (e.g., White and Dupré, 1986; Plank, 2014). Therefore, we explore the mixing relationships defined by mixing subduction zone processed subducted sediments and recycled oceanic crust (Stracke et al., 2003) into the depleted MORB mantle (DMM) for Pb isotopic compositions and Ce/Pb ratios. Yang et al. (2020) argue for a significant amount of recycled material (in a 95-5 % mixture of recycled oceanic crust

and upper continental crust material) mixed into the E-MORB source (e.g., 10 to 30 %). Such amounts of subducting sediment and recycled oceanic crust would decrease the Ce/Pb ratio and increase the $^{207}\text{Pb}/^{204}\text{Pb}$ ratio of the upper mantle source to unobserved compositions (Fig. 5). Recycling of a subducting sediment component, also has implications for the Mo and U isotopic compositions, and current combined Mo-U isotopic data on subducting sediment, and Mo data on metasediments are an unlikely candidate for creating E-MORB, with the meta-/sediment being too isotopically light in $\delta^{98/95}\text{Mo}$ (Freymuth et al., 2015; Ahmad et al., 2021) (Fig. 6, 7a). However, we note that sediment compositions can be variable (e.g., Freymuth et al., 2015; Ahmad et al., 2021) and that further characterisation of combined Mo-U isotopic data on subducted sediments is needed to show the potential influence of subducting sediments on the composition of the MORB source. Nonetheless, our inferences from global averaged Ce/Pb and Pb radiogenic compositions still preclude the mixing of subducted sediments into the E-MORB source (Fig. 5).

Other studies also suggest a role for recycled crustal material in the formation of E-MORB sources. Donnelly et al. (2004) argue for low degree partial melts of subducted oceanic crust as eclogite at depth that metasomatises the mantle wedge, creating necessary trace element enrichments. This material is subsequently recirculated through plate motion into the upper mantle over time, ≥ 300 Myr, to allow for radiogenic isotope ratio ingrowth, before being sampled again under MOR's in a larger degree melting event. Our data preclude this model, however, as the eclogitic residues of oceanic crust post subduction zone processing have isotopically light $\delta^{98/95}\text{Mo}$ and high Ce/Mo, which is not seen in E-MORB (Chen et al., 2019; Ahmad et al., 2021) (Fig. 7a). This is also likely the case for U given the compositions of volcanic arc lavas and AOC (Fig. 7b). Nielsen et al. (2018) suggest a similar model (i.e., two stage melting, with low degree melt metasomatism, and

radiogenic ingrowth followed by sampling under MOR's) but require the addition of subducted sediment, to fit with Ba isotopic data. However, as detailed above, subducted sediments in the E-MORB source are incompatible with Ce/Pb and Pb isotopic data of E-MORB (Fig. 5), as well as with Mo and U elemental and isotopic data (Fig. 6).

Some MORB samples with high “arc-like” $\delta^{98/95}\text{Mo}$, low $(\text{La}/\text{Sm})_{\text{N}}$, and other arc lava geochemical signatures have been linked to mantle sources with substantial contributions from fluid-modified mantle wedge components that formed during subduction processes such as enrichments in U and Pb that result in lower Nb/U (33) and Ce/Pb (19) (Chen et al., 2025) than canonical mantle values (47 ± 10 and 25 ± 5 respectively) (Hofmann et al., 1986). These MORB samples that preserve so called ghost-arc signatures reflect a way of generating high $\delta^{98/95}\text{Mo}$ in upper mantle MORB sources with recycled crustal components (Chen et al., 2025). However, our E-MORB samples with high $(\text{La}/\text{Sm})_{\text{N}}$ do not show evidence of arc lava signatures. For example they have average Nb/U (48) and Ce/Pb (28) near canonical mantle values (Hofmann et al., 1986). Therefore, the high $\delta^{98/95}\text{Mo}$ in our E-MORB samples cannot be explained by recycled fluid-modified mantle components.

The simplest interpretation of our new E-MORB data from the North Atlantic Ocean is that they do not contain a recycled, subduction zone processed, crustal component (Fig. 6, 7). Therefore, we argue for a model that does not invoke recycled crustal material to explain the Mo and U elemental and isotopic compositions of E-MORB samples.

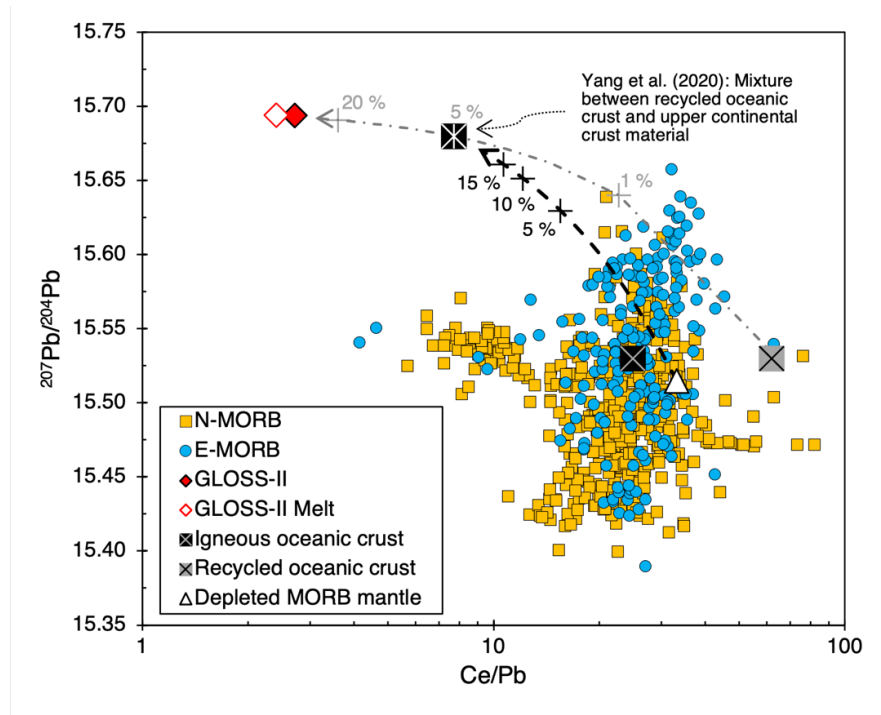


Fig. 5. Mixing model (dashed black line) for $^{207}\text{Pb}/^{204}\text{Pb}$ versus Ce/Pb between the depleted MORB mantle and subduction zone processed recycled oceanic crust mixed with recycled melted sediment (GLOSS-II, Plank, 2014) in a 95-5 % mixture following Yang et al. (2020) (dash-dotted grey line). Composition of recycled oceanic crust and melted subducted sediment composition have been calculated from Stracke et al. (2003). Mixing models have been calculated using parameters and sources in table S8. Filtered global MORB database from Gale et al. (2013) (only including data obtained by ICP-MS methods).

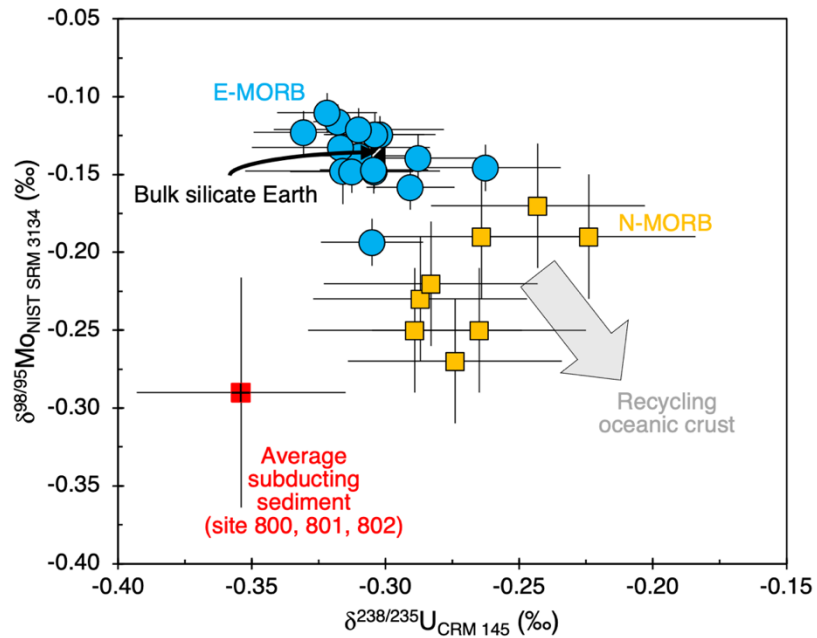


Fig. 6. $\delta^{238}\text{U}$ and $\delta^{98/95}\text{Mo}$ composition of E-MORB samples measured in this work (blue circles) and literature N-MORB (yellow squares) with U and Mo isotopic data. Symbols and sources for literature data are the same as used in figure 2. The grey arrow shows the effect of mixing recycled oceanic crust into the mantle, which does not explain composition of E-MORB relative to N-MORB.

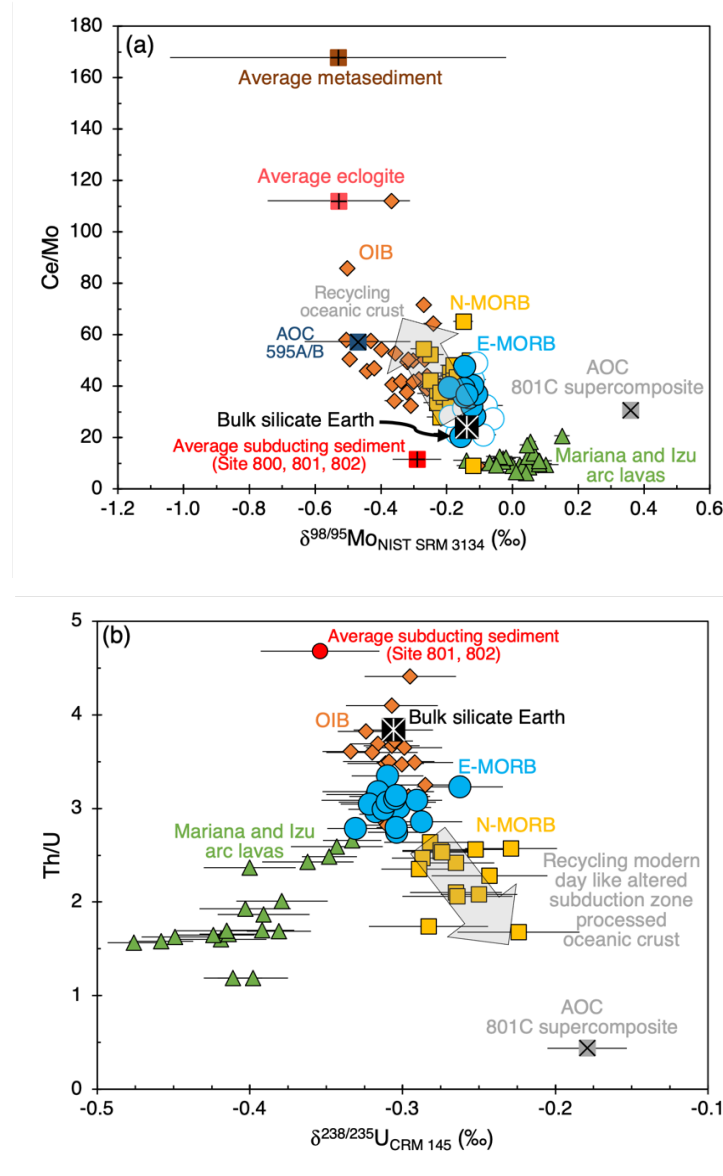


Fig. 7. (a) $\delta^{98/95}\text{Mo}$ and (b) $\delta^{238}\text{U}$ versus Ce/Mo and Th/U for N-MORB, E-MORB, AOC, Mariana and Izu arc lavas, OIB, eclogite, and subducting sediment and metasediment. Symbols and sources for literature data are the same as used in figure 2. Literature E-MORB data, shown as hollow blue circles, are from Bezard et al. (2016), Chen et al. (2022) and Hin et al. (2022). Grey arrows show the effect of mixing recycled oceanic crust into the upper mantle, which does not account for composition of E-MORB.

5.4 Low degree partial melting and mantle metasomatism

Low degree partial melting has been suggested to explain the incompatible element enrichment of fluid and non-fluid mobile elements in the E-MORB source (e.g., Niu et al., 2002). Uranium is highly incompatible during mantle melting, $D_{\text{Cpx/melt}} \text{U}^{4+} = \sim 0.02$ (Fonseca et al., 2014), and therefore, any potential isotopic fractionation between melt and initial source from partial melting of peridotite will be insignificant as virtually all U will enter the melt. The lower $\delta^{238}\text{U}$ of E-MORB than N-MORB can therefore not be explained by isotopic fractionation during partial melting. The $\delta^{238}\text{U}$ compositions of our E-MORB samples thus represent the compositions of their upper mantle sources. Their chondritic values reflect mantle compositions little- or un-affected by the recycling of AOC since the onset of oxic deep oceans (~ 600 Ma), which has been argued to increase the $\delta^{238}\text{U}$ of the upper mantle as sampled by N-MORB. We suggest that our $\delta^{238}\text{U}$ compositions of E-MORB can hence be explained by a model where ancient (≥ 600 Ma) mantle components are preserved and unaffected by more recent (< 600 Ma) crustal recycling.

This is compatible with a model of low degree partial melting and peridotite metasomatism, as outlined in Niu et al. (2002), and applied from a Mo isotopic perspective in Chen et al. (2022) and for other isotope systems such as Fe (e.g., Guo et al., 2023). Enriched domains in the upper mantle could exist as volumetrically minor lithologies of low degree melts dispersed as (frozen) dykes or veins in a depleted peridotitic matrix (Niu et al., 2002). Low degree melting may occur at the boundary between the thickening and cooling oceanic lithosphere and the asthenosphere. This region is marked by a low velocity zone (e.g., Green, 1971; Niu et al., 2002), which likely reflects the presence of small amounts of melt (e.g., Hirschmann, 2010). These small degree, low volume

melts would have low thermal inertia, and will freeze as they migrate into the base of the oceanic lithosphere (McKenzie, 1989). Such metasomatised lithosphere has also been invoked in the source of some alkaline lavas (e.g., Pilet et al., 2008). The existence of alkali volcanism with a chemistry that reflects small degree melting in the presence of garnet, far from any plate boundary or hot-spot in the north-western Pacific plate (Petit spots) (Hirano et al., 2006), has been used as evidence of small degree melts that are actively forming in the modern asthenosphere. The Petit spots anomalously result in a surface expression of this process due to lithospheric fractures from plate flexure during subduction allowing the melts to ascend (Hirano et al., 2006).

Uranium isotopic data of E-MORB samples requires that the initial low degree melting event happened ≥ 600 Ma, metasomatising the uppermost mantle and freezing in upper mantle compositions with enriched trace element compositions and chondritic $\delta^{238}\text{U}$. Thus, domains enriched in U are isolated from the evolution of ambient upper mantle to higher $\delta^{238}\text{U}$ by recycling of oceanic crust altered in oxic deep ocean conditions ($< 600\text{Ma}$). A full mechanistic explanation of the model of recycling and mixing of metasomatized oceanic lithosphere into the mantle is not the aim of our work and we refer readers to Niu (2002) and Niu and O'Hara (2003) for details. In brief, these metasomatised portions of the oceanic lithosphere would be subducted, and since they are in deep portions of lithosphere, they would not undergo dehydration. Heating of this material increases its buoyancy, and the crust and mantle separate by buoyancy contrast with crust sinking and thermally buoyant peridotitic mantle rising with metasomatised sections of dykes and veins (Niu et al., 2002; Niu and O'Hara, 2003). Such metasomatised lithosphere is stirred into the upper mantle but remains chemically distinct until ultimately sampled by melting beneath ridges to give rise to E-MORB (Fig. 8) (Niu et al., 2002; Niu and O'Hara, 2003).

711
712 Molybdenum isotope data of E-MORB are also compatible with such a model (Chen et al., 2022).
713 but unlike U, the Mo isotopic compositions of E-MORB may be fractionated from its source. In
714 pyroxene, the major upper mantle Mo host, Mo sits in the octahedral M1 site (Leitzke et al., 2017),
715 while in melt Mo^{6+} is coordinated tetrahedrally (Holzheid et al., 1994; O'Neill and Eggins, 2002;
716 Farges et al., 2006). While a minor species at modern ambient upper mantle oxygen fugacity,
717 Mo^{4+} is significantly less incompatible than Mo^{6+} in pyroxenes ($D_{\text{Cpx/melt}} \text{Mo}^{4+} = \sim 2$) (Leitzke et
718 al., 2017) and is coordinated octahedrally in both mineral and melt (Farges et al., 2006). Heavier
719 isotopes are concentrated in phases with stiffer and stronger bonds, which form between ions with
720 lower co-ordination number and higher valence state (e.g., Schauble, 2004). Melts are therefore
721 predicted to become isotopically heavier in Mo than residues during partial melting (McCoy-West
722 et al., 2019). The fractionation between Mo isotopes becomes larger at smaller degrees of melting
723 and lower $\text{Mo}^{6+}/\text{Mo}_T$ (Mo total) ratios (i.e., more reduced compositions, unlikely for modern
724 oxidised mantle) (Fig. S7a). Chen et al. (2022), following the melting models of McCoy-West et
725 al. (2019), proposed that at low degrees of melting, $\sim 0.2\%$, of modern-day depleted mantle,
726 $\delta^{98/95}\text{Mo} = -0.2\text{‰}$ (Hin et al., 2022), at a modern-day redox state, $\text{Mo}^{6+}/\text{Mo}_T = 0.99$ (O'Neill and
727 Eggins, 2002), results in a melt composition, $\delta^{98/95}\text{Mo} = \sim -0.01\text{‰}$ and $(\text{La}/\text{Sm})_N \sim 5.4$, that is
728 sufficient to explain the high $\delta^{98/95}\text{Mo}$ values and chemical enrichments seen in global E-MORB
729 when mixed with a depleted MORB component (Fig. 9a).

730
731 However, we find that with our new data on E-MORB the resulting isotopic compositions from
732 such low degree melting are too isotopically heavy to explain some of our data, even at higher
733 $\text{Mo}^{6+}/\text{Mo}_T$ ratios, ~ 0.999 (Fig. 9a). McCoy-West et al. (2019) used the 'ionic model' and literature

bond length data to derive a fractionation factor between ^{98}Mo and ^{95}Mo during mantle partial melting, $\alpha^{98/95}\text{Mo}_{\text{Melt-Silicate}}$, ~ 0.99977 . Such a value has not been directly, experimentally verified and notably predicts larger fractionation than for another redox sensitive system Cr (e.g., Jerram et al., 2022) for example. We note that our data imply a smaller melt-silicate fractionation of Mo isotopes, and we illustrate this using $\alpha^{98/95}\text{Mo}_{\text{Melt-Silicate}}$ of 0.9999 (Fig. S7b, 9b). Experimental work is required to assess if this empirical reassessment of the fractionation factor is justified.

Our model fit to $\delta^{98/95}\text{Mo}$ data is further improved given inferences from $\delta^{238}\text{U}$ compositions of E-MORB that imply the initial low degree melts form not from a modern-day depleted mantle, but ancient ≥ 600 Ma depleted mantle compositions (Fig. 8). Isotopic perturbation of Mo in the upper mantle by crustal recycling is inferred to have occurred for longer timescales than for U. Hin et al. (2022) show that at least ~ 1 to 1.4 Gyr of oceanic crust recycling is needed to lower the $\delta^{98/95}\text{Mo}$ value of the upper mantle from -0.14 ‰ (BSE) to -0.2 ‰ (modern-day depleted upper mantle). Although, as we note, if the melt-silicate fractionation of Mo isotope is smaller than estimated by McCoy-West et al. (2019), these timescales would be shorter, which is possible, as the U isotopic composition of N-MORB suggests that upper mantle compositions can be perturbed by recycled crust within 600 Myr. The isolation of small degree melts from a convecting upper mantle at various ages ≥ 600 Ma can help explain the variably elevated $\delta^{98/95}\text{Mo}$ of global E-MORB. We show this on fig. 9b, where low degree melt compositions form from an upper mantle less affected by crustal recycling with higher $\delta^{98/95}\text{Mo}$ than modern day, resulting in an enriched melt end member composition of $\delta^{98/95}\text{Mo} = \sim -0.1$ ‰ and $(\text{La}/\text{Sm})_{\text{N}} \sim 5.4$ at $\text{Mo}^{6+}/\text{Mo}_{\text{T}} = 0.99$.

In summary, the metasomatism of depleted, oceanic lithosphere with low degree melts formed ≥ 600 Ma would create a source dominated by a U-rich component with $\delta^{238}\text{U} \approx \text{BSE}$ and a range of $\delta^{98/95}\text{Mo}$ compositions $\geq \text{BSE}$, with variable enrichment in $(\text{La}/\text{Sm})_{\text{N}}$ (Fig. 8). Low degree melting would also create variable degrees of enrichment in other chemical tracers of enrichment, such as Nb/Zr, Th/Yb, and Sm/Nd, that also show trends with $\delta^{238}\text{U}$ and $\delta^{98/95}\text{Mo}$, that distinguish E-MORB from N-MORB (Fig. S8). This enriched component, when stirred back into the upper mantle and sampled by melting beneath a MOR in a larger degree melting event, can explain the chemical compositions of non-hot-spot influenced E-MORB (Fig. 3c, d, 9b). The timescale of ≥ 600 Ma inferred for this recycling process is about twice as long as the residence time of E-MORB sources calculated by Donnelly et al. (2004) from radiogenic isotope pseudo-chrons. It will be of interest to rationalise these different timescales using a consistent set of radiogenic isotope and $\delta^{238}\text{U}$ measurements on the same samples, which is currently not possible.

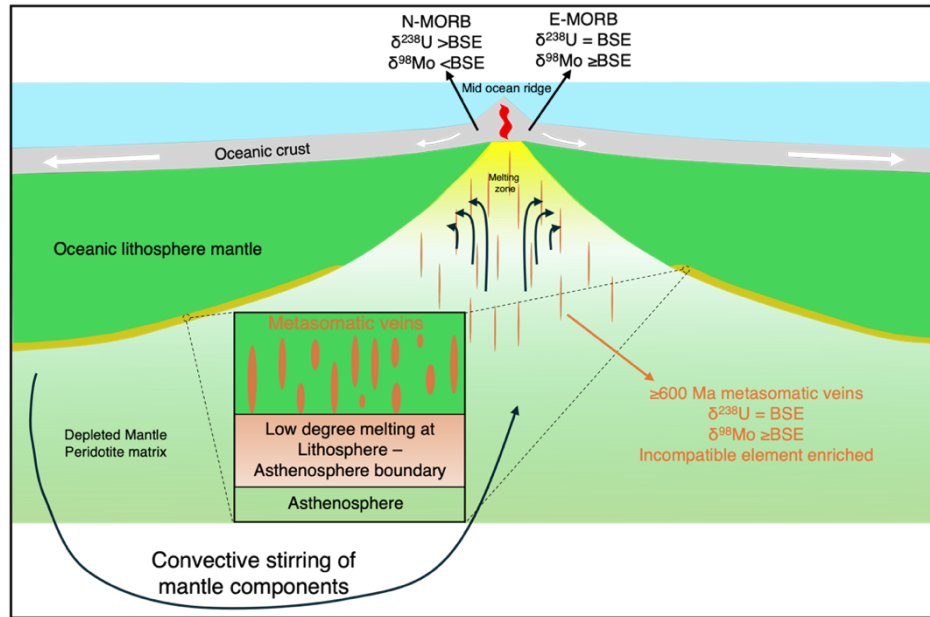


Fig. 8. Cartoon schematic of E-MORB source formation based on and modified from Niu et al. (2002) and Guo et al. (2023). Low degree partial melts enriched in incompatible elements (orange lenses) form ≥ 600 Ma in the low velocity zone at the boundary between the lithosphere and asthenosphere (shaded orange region at base of oceanic lithosphere mantle) and become trapped by migration and freezing in the cooling and thickening overlying oceanic lithosphere. These components preserve older mantle compositions with BSE $\delta^{238}\text{U}$. As oceanic lithosphere is subducted, the metasomatised lithosphere is stirred back into the upper mantle and some is entrained beneath MOR's and melts to produce E-MORB.

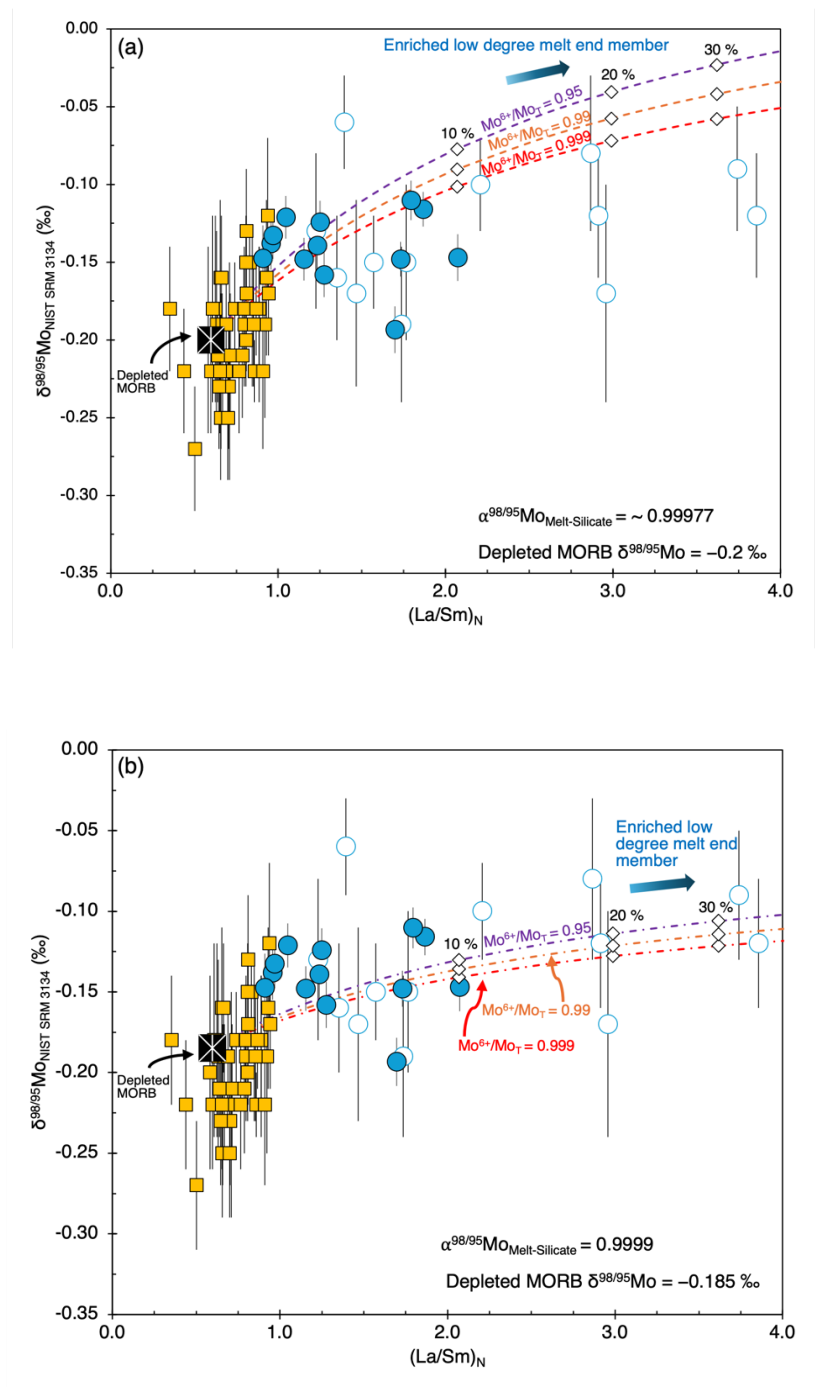


Fig. 9. Non-modal, batch melting modelling of $(\text{La}/\text{Sm})_{\text{N}}$ and Mo isotopic composition of melt. Mixing lines are shown between a depleted MORB (represented by 20 % melting of DMM) and an enriched low degree melt end member generated by 0.2 % melting of DMM at different mantle $f\text{O}_2$ ($\text{Mo}^{6+}/\text{Mo}_{\text{T}} = 0.999$ to 0.95). Symbols and sources for data are the same as used in figure 2. Model calculations follow McCoy-West et al. (2019) and Chen et al. (2022). Parameters used are given in table S9. White diamonds indicate mixing proportions. (a) $\alpha^{98/95}\text{Mo}_{\text{Melt-Silicate}} \sim 0.99977$, Depleted MORB $\delta^{98/95}\text{Mo} = -0.2 \text{ ‰}$ (b) $\alpha^{98/95}\text{Mo}_{\text{Melt-Silicate}} \sim 0.9999$, Depleted MORB $\delta^{98/95}\text{Mo} = -0.185 \text{ ‰}$.

6. Conclusions

A set of hand-picked E-MORB glasses from the Northern mid-Atlantic ridge picked to different degrees of stringency all have $^{234}\text{U}/^{238}\text{U}$ ratios close to secular equilibrium, indicating that samples likely reflect primary U and Mo isotopic composition. These E-MORB samples show a limited range of $\delta^{238}\text{U}$ and $\delta^{98/95}\text{Mo}$ from ~ -0.33 to -0.26 ‰ and -0.19 to -0.11 ‰ respectively and are both, on average, indistinguishable from the bulk silicate Earth (chondritic) U and Mo isotopic compositions. These E-MORB therefore have contrasting sources to modern N-MORB, which are super-chondritic in U and sub-chondritic in Mo isotope ratios, thought to be due to the recycling of modern day like subduction zone processed altered oceanic crust (Andersen et al., 2015; Hin et al., 2022). Our E-MORB data are inconsistent with models that explain their enrichment with recycled oceanic crust and or recycled sediment (e.g., Allège and Turcotte, 1986; Prinzhofer et al., 1989; Donnelly et al., 2004; Hémond et al., 2006; Waters et al., 2011; Ulrich et al., 2012; Nielsen et al., 2018; Yang et al., 2020) but are consistent with a model of recycled oceanic lithospheric mantle, metasomatised by small degree asthenosphere melts (Niu et al., 2002; Chen et al., 2022; Guo et al., 2023). This process effectively isolates the composition of the upper mantle at the time of the small degree melting until the metasomatised sources are resampled as E-MORB by melting beneath ridges. Uranium isotopic compositions (which are not affected by low degree partial melting) show that this initial low degree melting event occurred in an upper mantle with a chondritic $\delta^{238}\text{U}$, namely prior to its contamination with isotopically heavy recycled altered oceanic crust. This corresponds to an age ≥ 600 Ma, set by the estimated timing of deep ocean oxygenation (Andersen et al., 2015), providing a minimum bound on the antiquity of the E-MORB source. Molybdenum isotopic compositions of global E-MORB are compatible with such

870 a model but are also potentially fractionated during low degree partial melting to isotopically
871 heavier compositions (McCoy-West et al., 2019; Chen et al., 2022).

872

873

874

875

876

877

878

879

880

881

882

883

884

885

886

887

888

889

890

891

892

Credit authorship contribution statement

Joel B. Rodney: Data curation, formal analysis, investigation, methodology, validation, visualisation, writing – original draft. **Morten B. Andersen:** Supervision, project administration, funding acquisition, conceptualization, methodology, writing – review and editing. **Bramley J. Murton:** Resources, writing – review and editing. **Tim Elliott:** Supervision, project administration, funding acquisition, conceptualization, writing – review and editing.

Declaration of competing interest

The authors declare that they have no known competing financial interests or personal relationships that could have appeared to influence the work reported in this paper.

Data availability

Data are available through Mendeley data at:
<https://data.mendeley.com/datasets/wm84d8m8js/2>

Acknowledgments

JBR would like to acknowledge Christopher D. Coath and Carolyn Taylor for the upkeep of the labs. JBR would like to acknowledge Ian Parkinson, Paul Savage, and Shuo Chen for useful comments. JBR would like to thank Paolo A. Sossi for providing melting models. JBR would like

to thank Fang-Zhen Teng for editorial handling and Qasid Ahmad and one anonymous reviewer for helpful comments. JBR was supported by a NERC GW4 + Doctoral Training Partnership studentship from the Natural Environmental Research Council [NE/S007504/1]. JBR, MBA, and TE acknowledge funding from a NERC grant [NE/T012595/1 & NE/T012633/1]. RSS James Cook cruise JC024 expedition and project were funded by NERC award NE/C520598/1 (Roger Searle at Durham University) and NE/ C520612/1 (Bramley J Murton at the National Oceanography Centre).

Appendix A. Supplementary Material

Supplementary Material related to this article can be found online at:

References

- Ahmad, Q., M. Wille, S. König, C. Rosca, A. Hensel, T. Pettke, and J. Hermann, 2021, The Molybdenum isotope subduction recycling conundrum: A case study from the Tongan subduction zone, Western Alps and Alpine Corsica: *Chemical Geology*, **576**, 120231.
- Allègre, C. J., and D. L. Turcotte, 1986, Implications of a two-component marble-cake mantle: *Nature*, **323**, 123–127.
- Andersen, M. B., S. Romaniello, D. Vance, S. H. Little, R. Herdman, and T. W. Lyons, 2014, A modern framework for the interpretation of $^{238}\text{U}/^{235}\text{U}$ in studies of ancient ocean redox: *Earth and Planetary Science Letters*, **400**, 184–194.
- Andersen, M. B., T. Elliott, H. Freymuth, K. W. W. Sims, Y. Niu, and K. A. Kelley, 2015, The terrestrial uranium isotope cycle: *Nature*, **517**, 356–359.
- Andersen, M. B., J. B. Rodney, H. Freymuth, F. Vils, M. Harris, K. Cooper, D. A. H. Teagle, and T. Elliott, 2024, Time scales and mechanisms of uranium uptake in altered ocean crust: observations from the ~15 million year-old site 1256 in the eastern equatorial Pacific: *Geochimica et Cosmochimica Acta*, **382**, 142–159.
- Bezard, R., M. Fischer-Gödde, C. Hamelin, G. A. Brenneka, and T. Kleine, 2016, The effects of magmatic processes and crustal recycling on the molybdenum stable isotopic composition of Mid-Ocean Ridge Basalts: *Earth and Planetary Science Letters*, **453**, 171–181.
- Bougault, H., L. Dmitriev, J. G. Schilling, A. Sobolev, J. L. Joron, and H. D. Needham, 1988, Mantle heterogeneity from trace elements: MAR triple junction near 14°N: *Earth and Planetary Science Letters*, **88**, 27–36.
- Burkhardt, C., R. C. Hin, T. Kleine, and B. Bourdon, 2014, Evidence for Mo isotope fractionation in the solar nebula and during planetary differentiation: *Earth and Planetary Science Letters*, **391**, 201–211.
- Chen, S., P. Sun, Y. Niu, P. Guo, T. Elliott, and R. C. Hin, 2022, Molybdenum isotope systematics of lavas from the East Pacific Rise: Constraints on the source of enriched mid-ocean ridge basalt: *Earth and Planetary Science Letters*, **578**, 117283.

967 Chen, S., R. C. Hin, T. John, R. Brooker, B. Bryan, Y. Niu, and T. Elliott, 2019, Molybdenum
 968 systematics of subducted crust record reactive fluid flow from underlying slab serpentine
 969 dehydration: *Nature Communications*, **10**, 4773.

970 Chen, Z., F.-Z. Teng, R. J. Stern, Y. Zhang, J. Li, and Z. Zeng, 2025, Molybdenum isotope evidence
 971 for subduction-modified mantle beneath mid-ocean ridges: *Earth and Planetary Science*
 972 *Letters*, **658**, 119294.

973 Cheng, H., R. Lawrence Edwards, C.-C. Shen, V. J. Polyak, Y. Asmerom, J. Woodhead, J.
 974 Hellstrom, Y. Wang, X. Kong, C. Spötl, X. Wang, and E. Calvin Alexander, 2013,
 975 Improvements in ^{230}Th dating, ^{230}Th and ^{234}U half-life values, and U–Th isotopic
 976 measurements by multi-collector inductively coupled plasma mass spectrometry: *Earth and*
 977 *Planetary Science Letters*, **371–372**, 82–91.

978 Collerson, K. D., and B. S. Kamber, 1999, Evolution of the Continents and the Atmosphere
 979 Inferred from Th-U-Nb Systematics of the Depleted Mantle: *Science*, **283**, 1519–1522.

980 Donnelly, K. E., S. L. Goldstein, C. H. Langmuir, and M. Spiegelman, 2004, Origin of enriched
 981 ocean ridge basalts and implications for mantle dynamics: *Earth and Planetary Science*
 982 *Letters*, **226**, 347–366.

983 Elliott, T., A. Zindler, and B. Bourdon, 1999, Exploring the kappa conundrum: the role of recycling
 984 in the lead isotope evolution of the mantle: *Earth and Planetary Science Letters*, **169**, 129–
 985 145.

986 Farges, F., R. Siewert, G. Brown, A. Guesdon, and G. Morin, 2006, Structural Environments
 987 Around Molybdenum in Silicate Glasses and Melts. I. Influence of Composition and
 988 Oxygen Fugacity on the Local Structure of Molybdenum: *Canadian Mineralogist*, **44**, 731–
 989 753.

990 Fonseca, R. O. C., G. Mallmann, P. Sprung, J. E. Sommer, A. Heuser, I. M. Speelmanns, and H.
 991 Blanchard, 2014, Redox controls on tungsten and uranium crystal/silicate melt partitioning
 992 and implications for the U/W and Th/W ratio of the lunar mantle: *Earth and Planetary*
 993 *Science Letters*, **404**, 1–13.

994 Freymuth, H., M. B. Andersen, and T. Elliott, 2019, Uranium isotope fractionation during slab
 995 dehydration beneath the Izu arc: *Earth and Planetary Science Letters*, **522**, 244–254.

996 Freymuth, H., F. Vils, M. Willbold, R. N. Taylor, and T. Elliott, 2015, Molybdenum mobility and
 997 isotopic fractionation during subduction at the Mariana arc: *Earth and Planetary Science*
 998 *Letters*, **432**, 176–186.

999 Gale, A., C. A. Dalton, C. H. Langmuir, Y. Su, and J.-G. Schilling, 2013, The mean composition
 1000 of ocean ridge basalts: *Geochemistry, Geophysics, Geosystems*, **14**, 489–518.

1001 Gaschnig, R. M., C. T. Reinhard, N. J. Planavsky, X. Wang, D. Asael, and C. Chauvel, 2017, The
 1002 Molybdenum Isotope System as a Tracer of Slab Input in Subduction Zones: An Example
 1003 From Martinique, Lesser Antilles Arc: *Geochemistry, Geophysics, Geosystems*, **18**, 4674–
 1004 4689.

1005 Goto, K. T., A. D. Anbar, G. W. Gordon, S. J. Romaniello, G. Shimoda, Y. Takaya, A. Tokumaru,
 1006 T. Nozaki, K. Suzuki, S. Machida, T. Hanyu, and A. Usui, 2014, Uranium isotope
 1007 systematics of ferromanganese crusts in the Pacific Ocean: Implications for the marine 238
 1008 $U/^{235}U$ isotope system: *Geochimica et Cosmochimica Acta*, **146**, 43–58.

1009 Green, D. H., 1971, Composition of Basaltic Magmas as Indicators of Conditions of Origin:
 1010 Application to Oceanic Volcanism: *Philosophical Transactions of the Royal Society of*
 1011 *London Series A*, **268**, 707–722.

1012 Guo, P., Y. Niu, S. Chen, M. Duan, P. Sun, Y. Chen, H. Gong, and X. Wang, 2023, Low-degree
 1013 melt metasomatic origin of heavy Fe isotope enrichment in the MORB mantle: *Earth and*
 1014 *Planetary Science Letters*, **601**, 117892.

1015 Gutjahr, M., M. Frank, C. H. Stirling, V. Klemm, T. van de Flierdt, and A. N. Halliday, 2007,
 1016 Reliable extraction of a deepwater trace metal isotope signal from Fe–Mn oxyhydroxide
 1017 coatings of marine sediments: *Chemical Geology*, **242**, 351–370.

1018 Halliday, A. N., D.-C. Lee, S. Tommasini, G. R. Davies, C. R. Paslick, J. Godfrey Fitton, and D.
 1019 E. James, 1995, Incompatible trace elements in OIB and MORB and source enrichment in
 1020 the sub-oceanic mantle: *Earth and Planetary Science Letters*, **133**, 379–395.

1021 Hémond, C., A. W. Hofmann, I. Vlastélic, and F. Nauret, 2006, Origin of MORB enrichment and
 1022 relative trace element compatibilities along the Mid-Atlantic Ridge between 10° and 24°N:
 1023 *Geochemistry, Geophysics, Geosystems*, **7**, Q12010.

1024 Henderson, G. M., and K. W. Burton, 1999, Using ($^{234}U/^{238}U$) to assess diffusion rates of isotope
 1025 tracers in ferromanganese crusts: *Earth and Planetary Science Letters*, **170**, 169–179.

1026 Hin, R. C., K. E. J. Hibbert, S. Chen, M. Willbold, M. B. Andersen, E. S. Kiseeva, B. J. Wood, Y.
 1027 Niu, K. W. W. Sims, and T. Elliott, 2022, The influence of crustal recycling on the
 1028 molybdenum isotope composition of the Earth's mantle: *Earth and Planetary Science*
 1029 *Letters*, **595**, 117760.

1030 Hirano, N., E. Takahashi, J. Yamamoto, N. Abe, S. P. Ingle, I. Kaneoka, T. Hirata, J.-I. Kimura, T.
 1031 Ishii, Y. Ogawa, S. Machida, and K. Suyehiro, 2006, Volcanism in Response to Plate
 1032 Flexure: *Science*, **313**, 1426–1428.

1033 Hirschmann, M. M., 2010, Partial melt in the oceanic low velocity zone: *Physics of the Earth and*
 1034 *Planetary Interiors*, **179**, 60–71.

1035 Hofmann, A. W., K. P. Jochum, M. Seufert, and W. M. White, 1986, Nb and Pb in oceanic basalts:
 1036 new constraints on mantle evolution: *Earth and Planetary Science Letters*, **79**, 33–45.

1037 Holzheid, A., A. Borisov, and H. Palme, 1994, The effect of oxygen fugacity and temperature on
 1038 solubilities of nickel, cobalt, and molybdenum in silicate melts: *Geochimica et*
 1039 *Cosmochimica Acta*, **58**, 1975–1981.

1040 Jerram, M., P. Bonnand, J. Harvey, D. Ionov, and A. N. Halliday, 2022, Stable chromium isotopic
 1041 variations in peridotite mantle xenoliths: *Metasomatism versus partial melting:*
 1042 *Geochimica et Cosmochimica Acta*, **317**, 138–154.

1043 Kipp, M. A., H. Li, M. J. Ellwood, S. G. John, R. Middag, J. F. Adkins, and F. L. H. Tissot, 2022,
 1044 ^{238}U , ^{235}U and ^{234}U in seawater and deep-sea corals: A high-precision reappraisal:
 1045 *Geochimica et Cosmochimica Acta*, **336**, 231–248.

1046 König, S., M. Wille, A. Voegelin, and R. Schoenberg, 2016, Molybdenum isotope systematics in
 1047 subduction zones: *Earth and Planetary Science Letters*, **447**, 95–102.

1048 Kostopoulos, D., K., and B. Murton J., 1992, Origin and distribution of components in boninite
 1049 genesis: significance of the OIB component: Geological Society, London, Special
 1050 Publications, **60**, 133–154.

1051 Leitzke, F. P., R. O. C. Fonseca, P. Sprung, G. Mallmann, M. Lagos, L. T. Michely, and C. Münker,
 1052 2017, Redox dependent behaviour of molybdenum during magmatic processes in the
 1053 terrestrial and lunar mantle: Implications for the Mo/W of the bulk silicate Moon: *Earth*
 1054 *and Planetary Science Letters*, **474**, 503–515.

- Liang, Y.-H., A. N. Halliday, C. Siebert, J. G. Fitton, K. W. Burton, K.-L. Wang, and J. Harvey, 2017, Molybdenum isotope fractionation in the mantle: *Geochimica et Cosmochimica Acta*, **199**, 91–111.
- Lyons, T. W., C. T. Reinhard, and N. J. Planavsky, 2014, The rise of oxygen in Earth's early ocean and atmosphere: *Nature*, **506**, 307–315.
- Maia, M., J. Goslin, and P. Gente, 2007, Evolution of the accretion processes along the Mid-Atlantic Ridge north of the Azores since 5.5 Ma: An insight into the interactions between the ridge and the plume: *Geochemistry, Geophysics, Geosystems*, **8**, Q03013.
- McCoy-West, A. J., P. Chowdhury, K. W. Burton, P. Sossi, G. M. Nowell, J. G. Fitton, A. C. Kerr, P. A. Cawood, and H. M. Williams, 2019, Extensive crustal extraction in Earth's early history inferred from molybdenum isotopes: *Nature Geoscience*, **12**, 946–951.
- McCulloch, M. T., 1993, The role of subducted slabs in an evolving Earth: *Earth and Planetary Science Letters*, **115**, 89–100.
- McDonough, W. F., and S. -s Sun, 1995, The composition of the Earth: *Chemical Geology*, **120**, 223–253.
- McKenzie, D., 1989, Some remarks on the movement of small melt fractions in the mantle: *Earth and Planetary Science Letters*, **95**, 53–72.
- Nielsen, S. G., T. J. Horner, H. V. Pryer, J. Blusztajn, Y. Shu, M. D. Kurz, and V. Le Roux, 2018, Barium isotope evidence for pervasive sediment recycling in the upper mantle: *Science Advances*, **4**, eaas8675.
- Niu, Y., and M. J. O'Hara, 2003, Origin of ocean island basalts: A new perspective from petrology, geochemistry, and mineral physics considerations: *Origin of ocean island basalts: Journal of Geophysical Research: Solid Earth*, **108**, 2209.
- Niu, Y., M. Regelous, I. J. Wendt, R. Batiza, and M. J. O'Hara, 2002, Geochemistry of near-EPR seamounts: importance of source vs. process and the origin of enriched mantle component: *Earth and Planetary Science Letters*, **199**, 327–345.
- O'Neill, H. St. C., and S. M. Eggins, 2002, The effect of melt composition on trace element partitioning: an experimental investigation of the activity coefficients of FeO, NiO, CoO, MoO₂ and MoO₃ in silicate melts: *Chemical Geology*, **186**, 151–181.
- Pilet, S., M. B. Baker, and E. M. Stolper, 2008, Metasomatized Lithosphere and the Origin of Alkaline Lavas: *Science*, **320**, 916-919.

1086 Plank, T., 2014, 4.17 - The Chemical Composition of Subducting Sediments, *in* H. D. Holland and
1087 K. K. Turekian, eds., *Treatise on Geochemistry* (Second Edition), Elsevier, 607–629.

1088 Prinzhofer, A., E. Lewin, and C. J. Allègre, 1989, Stochastic melting of the marble cake mantle:
1089 evidence from local study of the East Pacific Rise at 12°50'N: *Earth and Planetary Science*
1090 *Letters*, **92**, 189–206.

1091 Reinitz, I., and K. K. Turekian, 1989, ²³⁰Th/²³⁸U and ²²⁶Ra/²³⁰Th fractionation in young
1092 basaltic glasses from the East Pacific Rise: *Earth and Planetary Science Letters*, **94**, 199–
1093 207.

1094 Richter, S., A. Alonso-Munoz, R. Eykens, U. Jacobsson, H. Kuehn, A. Verbruggen, Y. Aregbe, R.
1095 Wellum, and E. Keegan, 2008, The isotopic composition of natural uranium samples -
1096 Measurements using the new n(²³³U)/n(²³⁶U) double spike IRMM-3636: *International*
1097 *Journal of Mass Spectrometry*, **269**, 145–148.

1098 Schauble, E. A., 2004, Applying Stable Isotope Fractionation Theory to New Systems: Reviews in
1099 *Mineralogy and Geochemistry*, **55**, 65–111.

1100 Schilling, J. G., G. Thompson, R. Kingsley, and S. Humphris, 1985, Hotspot—migrating ridge
1101 interaction in the South Atlantic: *Nature*, **313**, 187–191.

1102 Schilling, J.-G., 1975, Rare-Earth variations across ‘normal segments’ of the Reykjanes Ridge,
1103 60°-53°N, Mid-Atlantic Ridge, 29°S, and East Pacific Rise, 2°-19°S, and evidence on the
1104 composition of the underlying low-velocity layer: *Journal of Geophysical Research*, **80**,
1105 1459–1473.

1106 Searle, R. C., B. J. Murton, K. Achenbach, T. LeBas, M. Tivey, I. Yeo, M. H. Cormier, J. Carlut,
1107 P. Ferreira, C. Mallows, K. Morris, N. Schroth, P. van Calsteren, and C. Waters, 2010,
1108 Structure and development of an axial volcanic ridge: Mid-Atlantic Ridge, 45°N: *Earth and*
1109 *Planetary Science Letters*, **299**, 228–241.

1110 Siebert, C., T. F. Nägler, F. von Blanckenburg, and J. D. Kramers, 2003, Molybdenum isotope
1111 records as a potential new proxy for paleoceanography: *Earth and Planetary Science*
1112 *Letters*, **211**, 159–171.

1113 Staudigel, H., G. R. Davies, S. R. Hart, K. M. Marchant, and Brian. M. Smith, 1995, Large scale
1114 isotopic Sr, Nd and O isotopic anatomy of altered oceanic crust: DSDP/ODP sites 417/418:
1115 *Earth and Planetary Science Letters*, **130**, 169–185.

- Stracke, A., M. Bizimis, and V. J. M. Salters, 2003, Recycling oceanic crust: Quantitative constraints: *Geochemistry, Geophysics, Geosystems*, **4**, 8003.
- Ulrich, M., C. Hémond, P. Nonnotte, and K. P. Jochum, 2012, OIB/seamount recycling as a possible process for E-MORB genesis: *Geochemistry, Geophysics, Geosystems*, **13**, Q0AC19.
- Villalobos-Orchard, J., H. Freymuth, B. O'Driscoll, T. Elliott, H. Williams, M. Casalini, and M. Willbold, 2020, Molybdenum isotope ratios in Izu arc basalts: The control of subduction zone fluids on compositional variations in arc volcanic systems: *Geochimica et Cosmochimica Acta*, **288**, 68–82.
- Waters, C. L., K. W. W. Sims, M. R. Perfit, J. Blichert-Toft, and J. Blusztajn, 2011, Perspective on the Genesis of E-MORB from Chemical and Isotopic Heterogeneity at 9–10°N East Pacific Rise: *Journal of Petrology*, **52**, 565–602.
- White, W. M., and B. Dupré, 1986, Sediment subduction and magma genesis in the Lesser Antilles: Isotopic and trace element constraints: *Journal of Geophysical Research: Solid Earth*, **91**, 5927–5941.
- Willbold, M., and T. Elliott, 2023, Molybdenum isotope evidence for subduction-modified, recycled mafic oceanic crust in the mantle sources of ocean island basalts from La Palma and Hawaii: *Earth and Planetary Science Letters*, **621**, 118399.
- Willbold, M., K. Hibbert, Y.-J. Lai, H. Freymuth, R. C. Hin, C. Coath, F. Vils, and T. Elliott, 2016, High-Precision Mass-Dependent Molybdenum Isotope Variations in Magmatic Rocks Determined by Double-Spike MC-ICP-MS: *Geostandards and Geoanalytical Research*, **40**, 389–403.
- Wilson, S. C., B. J. Murton, and R. N. Taylor, 2013, Mantle composition controls the development of an Oceanic Core Complex: *Geochemistry, Geophysics, Geosystems*, **14**, 979–995.
- Yang, S., M. Humayun, and V. J. M. Salters, 2020, Elemental constraints on the amount of recycled crust in the generation of mid-oceanic ridge basalts (MORBs): *Science Advances*, **6**, eaba2923.
- Zartman, R. E., and S. M. Haines, 1988, The plumbotectonic model for Pb isotopic systematics among major terrestrial reservoirs - A case for bi-directional transport: *Geochimica et Cosmochimica Acta*, **52**, 1327–1339.

Constraints from uranium and molybdenum isotope ratios on the origin of enriched mid-ocean ridge basalts

Joel B. Rodney^{a*}, Morten B. Andersen^b, Bramley J. Murton^c, Tim Elliott^a

^aBristol Isotope Group, School of Earth Sciences, University of Bristol, Wills Memorial Building, Queen's Road, Bristol, BS8 1RJ, UK

^bSchool of Earth & Environmental Sciences, Cardiff University, Park Place, Cardiff, CF10 3AT, UK

^cNational Oceanography Centre, Waterfront Campus, European Way, Southampton, SO14 3ZH, UK

*Corresponding author

Email addresses: joel.rodney@bristol.ac.uk (J.B. Rodney), andersenm1@cardiff.ac.uk (M.B. Andersen), bramley.murton@noc.ac.uk (B.J. Murton), tim.elliott@bristol.ac.uk (T. Elliott).

1177 **Supplementary Information**

1178 Section 1: MORB glass picking and leaching

1179 Section 2: Full detailed method for U and Mo isotopic analysis

1180 Section 3: Supplementary figures and tables

1181

1182

1183

1184

1185

1186

1187

1188

1189

1190

1191

1192

1193

1194

1195

1196

1197

1198

1199

1200

Section 1:

MORB glass picking and leaching

Hand specimen samples of E-MORB were crushed and processed to $\sim 1000\ \mu\text{m}$ size glass chips. Glass chips were further crushed using an agate pestle and mortar, and sieved, aiming for a size of $\sim 600\ \mu\text{m}$. Mid-ocean ridge basalt glasses potentially experience seawater alteration, including Fe–Mn coatings precipitated on their surfaces, which can contain high concentrations of Mo and U. For example, it has been shown that the inclusion of Fe-Mn coatings that have high Mo contents $\sim 450\ \text{ug g}^{-1}$, with extremely fractionated Mo isotopic compositions, $\delta^{98/95}\text{Mo} -2\ \text{‰}$ (Siebert et al., 2003) can decrease $\delta^{98/95}\text{Mo}$ up to $\sim 0.07\ \text{‰}$ (Hin et al., 2022).

To avoid this, MORB glass samples were hand-picked under a binocular microscope to ensure samples were optically clear and devoid of any potential alteration. While this process has long been employed in various studies of MORB glass, notably in U-series disequilibrium studies (Reinitz and Turekian, 1989; Bourdon et al., 2000), it is laborious, and considering the large quantities of sample often needed for trace element isotopic analysis (e.g., $>1\ \text{g}$), a rate limiting step. Hand picking MORB glass can also be a relatively subjective task, and therefore it is unclear exactly what an acceptable limit of “quality” is.

A reliable check of sample alteration is given by $^{234}\text{U}/^{238}\text{U}$ activity ratios. If unaltered by any recent seawater alteration (that would likely affect U compositions), the ^{238}U decay chain will be in secular equilibrium, and so the activity ratio of ($^{234}\text{U}/^{238}\text{U}$), will be at unity. Seawater has ($^{234}\text{U}/^{238}\text{U}$) ~ 1.14 (Kipp et al., 2022) and so elevated ($^{234}\text{U}/^{238}\text{U}$) in glass samples indicates addition of seawater U onto Fe/Mn coatings, which could also indicate adsorption of isotopically distinctive Mo. We explore the effect of varyingly stringent picking strategies on samples with abundant glass. Different splits of glass, classed A, B, C, and D in decreasing degree of quality were prepared. Samples of quality A is those that are most optically clear and devoid of all alteration and coatings (Fig. S1). Samples of quality B is less optically clear, but still mostly devoid of alteration and coatings (Fig. S1). Samples of quality C is even less optically clear or have inclusions and minor amounts of coatings (Fig. S1). Glass quality D, with large amounts of inclusions, coatings or noticeably different to the bulk sample was rejected and not measured (Fig. S1). While this

increased sample preparation time, it does potentially increase the amount of measurable sample and allows an investigation into how selective MORB glass picking needs to be. The amounts of glass picked for each quality (A, B or C) for each sample varied and are listed in table S7. In some cases, different splits were combined to ensure there was enough sample to measure.

All samples underwent a reductive leaching step prior to dissolution to remove any Fe-Mn coatings that picking had failed to exclude. Picked glass samples were poured into 12 ml centrifuge tubes and rinsed thrice with $>18\text{ M } \Omega\cdot\text{cm}$ water (hereafter milli-Q water). Samples were shaken vigorously overnight using a vortex shaker with a 10 ml mixture of 0.05 M hydroxylamine hydrochloride, 15 % acetic acid and 0.03 M Na-EDTA buffered to pH 4 with NaOH (Gutjahr et al., 2007). The leachate was collected, and samples rinsed thrice with 10 ml milli-Q water that was also added to the collected leachate solution. Collected leachate solutions were analysed in 0.3 M HNO_3 for elemental concentrations using an ICP-MS Element2, at the University of Bristol. As noted by Andersen et al. (2015) and Hin et al. (2022) leaching can result in small amounts of glass dissolution, and thus U and Mo loss. Ratios of the concentrations of elements that absorb to Fe-Mn coatings e.g., U and Mo to those little affected, such as Th, Sc, Ti, and Zr, that would only be removed during glass dissolution, were monitored to examine the effects of leaching.

Uranium and Mo are removed during the leaching process (Fig. S2), and it is possible that the removed U and Mo is either from secondary coatings (Fe-Mn coatings) or from the dissolution of the MORB glass. Three leachates from MORB glass sample JC24-82-21, glass qualities A, B and C were measured before leaching other MORB samples to test the leaching procedure. Uranium was lost mostly in the first leaching step on all qualities of glass, $\sim 10\%$ loss, with then only 1 % or less lost in leaching steps 2 and 3 (Fig. S2). This was associated with systematic changes in U/Th of the leachates (Fig. S3). Comparing U to less mobile elements such as Th (which is only likely to be released during glass dissolution) shows the effects of the leaching procedure (Fig. S3). In the first leachate (sample JC24-82-21) U/Th are elevated, e.g., $\text{U/Th} > 4$, and likely reflects the release of secondary coating hosted U (Fig. S3). In the second and third leachates, these ratios all drop, e.g., $\text{U/Th} < 2$ and show little change between leach two and three (Fig. S3). This likely reflects only small amounts of U being released, also seen in the similar amount of U loss compared to the bulk sample in leachates 2 and 3 (Fig. S2). Given the large change between the first and

second leaches seen and the little variation between the second and third, it seems reasonable that one to two leaching steps are enough to remove any potential secondary coatings. We used two leaching steps for other samples but note that one is likely sufficient.

When comparing the rest of the data set, for which only two leaching steps were done, similar trends are seen for the amounts of U and Mo loss. For Mo, however, leaching loss is more consistently <5 % and is relatively consistent between leaching steps (Fig. S2). This suggests very little secondary phase hosted Mo, which should be removed in the first leach (as for U), and minimal glass dissolution. The main concern with the leaching process is that it may alter isotopic compositions, however Andersen et al. (2015) and Hin et al. (2022) show that the leaching procedure does not fractionate U or Mo isotopes of fresh glass, from comparing a leached and unleached BHVO glass sample. Therefore, even if some of U and Mo loss is from glass dissolution rather than the dissolution of secondary coatings, isotopic compositions should not be perturbed.

Leaching all the different qualities of glass picked for a sample allows us to compare if lower quality glass (e.g., C quality) as determined visually had more secondary alteration. However, all different qualities of glass showed largely the same patterns in U and Mo loss (Fig. S2, S3). Given this, our screening for glass quality may have been too broad, i.e., what we assessed as quality C (lowest measured quality), may have been just as high enough quality as quality B or A. This is further seen in the largely indistinguishable isotopic compositions of MORB glass samples of different quality (Fig. S5).

The $\delta^{234}\text{U}$ compositions of different qualities of glass picked and leached for each sample, A, B and C (in decreasing order of perceived quality), was used to assess the acceptable quality limit to use in future sampling of quenched MORB glass. The $\delta^{238}\text{U}$ compositions of the different qualities of glass picked and leached are all, bar one sample, within analytical uncertainty (Fig. S5a) and bar JC24-89-13, are also within uncertainty of $\delta^{234}\text{U} = 0$ (Fig. S5b). Sample JC24-89-13, which is only elevated above 0 by 2.5 ‰ in $\delta^{234}\text{U}$ (Fig. S5b), also has a similar $\delta^{238}\text{U}$ to other samples (Fig. S5a). The $\delta^{98/95}\text{Mo}$ compositions of different qualities of MORB glass are also all within analytical uncertainty (Fig. S5c). For samples with multiple splits, the fact that different qualities of glass are all within secular equilibrium and within uncertainty of one another has two important benefits:

firstly, it allows us to assess the level of MORB glass quality needed to ensure minimal secondary alteration, i.e., quality C; secondly, we can average all the splits (A, B, and C) for individual samples for overall $\delta^{238}\text{U}$, $\delta^{234}\text{U}$, and $\delta^{98/95}\text{Mo}$ compositions (Table S6, S7). This approach is reasonable given that the majority of samples with different splits (A, B, and C) have $\delta^{238}\text{U}$ and $\delta^{98/95}\text{Mo}$ compositions largely indistinguishable from one another (Fig. S5a, c).

Section 2:

Full detailed method for U and Mo isotopic analysis

For the U isotopic measurements, sample preparation and analysis followed Andersen et al. (2015) with some modification, and for Mo isotopic measurement followed Willbold et al. (2016) and Hin et al. (2022).

Uranium and Mo isotope analysis was conducted in the University of Bristol, Bristol isotope group labs. Approximately 1 g of MORB glass was digested in pre-cleaned Teflon PFA beakers in ~ 24 ml of acid using a mixture of 5:1 15.6 M HNO₃ and Romil UpA 28.1 M HF and placed on a tabletop hotplate at 120 °C for at least 48 hours. Samples were then evaporated to dryness and re-dissolved twice in 6 M HCl to remove fluoride precipitates and achieve full sample dissolution. The double spike tracer, IRMM3636 ²³⁶U – ²³³U, 50:50 (Richter et al., 2008), was added to samples prior to dissolution. The double spike was added to samples according to their U concentrations aiming for a ²³⁶U/²³⁵U ratio of 5. Samples were also spiked with a ⁹⁷Mo – ¹⁰⁰Mo double spike, prepared by the Bristol Isotope group, with a ⁹⁷Mo/⁹⁵Mo ratio of 47.58 and ¹⁰⁰Mo/⁹⁵Mo ratio of 58.32, aiming for a natural Mo-double spike Mo proportion of 0.5. For measurement of Th, U, and Mo, concentrations (non-isotope dilution), small fractions of samples (~ 1 %) were taken and measured on an Element2 at the University of Bristol following Andersen et al. (2014). Measured concentrations of U, Th, and Mo of reference materials measured on the Element2 are in good agreement with literature values (Table S2).

Samples were first processed for U isotopic analysis. Samples were loaded in 40 ml of 1.5 M HNO₃ onto 1 ml of TRU resin (100 – 150 mesh) in commercially available Bio-Rad Poly-Prep columns. Matrix was eluted in 30 ml of 1.5 M HNO₃, before U was collected in 10 ml of 0.3 M HF – 0.1 M HCl. The 40 ml of sample load and first 10 ml of wash was collected and kept for Mo chemistry. Collected U fractions were dried and fluxed in a 1 ml 50:50 15.6 M HNO₃: 30 % Romil SpA H₂O₂ mixture to eliminate any organic material that may have leached off resin into samples. Samples were loaded in 5 ml 3 M HNO₃ onto 0.5 ml of UTEVA resin (100 – 150 mesh), for Th and U separation, with 10 ml of 3 M HNO₃ washed through to elute any residual matrix, before washing through 15 ml of 5 M HCl to elute Th, before collection of U in 6 ml of 0.3 M HF – 0.1

M HCl. Again, any potential organic material was eliminated from samples. Final U collections were then dried and re-dissolved in a requisite amount of 0.2 M HCl (aiming for U concentration of 100 – 300 ng g⁻¹) for isotopic analysis. This procedure achieved efficient removal of Th and Th/U ratios during isotopic analysis were typically <0.005.

Uranium isotope compositions were measured on a ThermoFinnigan Neptune MC-ICP-MS (serial no. 1002) at the Bristol Isotope group in low mass resolution ($M/\Delta M \sim 2000$, 5 to 95 % peak height definition), using the setup detailed in Andersen et al. (2015). Samples were introduced to the plasma using a $\sim 40 \text{ ul min}^{-1}$ micro-concentric PFA nebuliser connected to a Cetac Aridus (1st generation) desolvating system. A standard sample cone plus X-skimmer cone set up was used. Masses 232 (²³²Th), 233 (²³³U), 234 (²³⁴U), 235 (²³⁵U), 236 (²³⁶U), and 238 (²³⁸U) were collected in faraday cups, with most cups connected to feedback amplifiers with $10^{11} \Omega$ resistors, apart from 234 which was connected to a $10^{13} \Omega$ resistor and 238 which was connected to a $10^{10} \Omega$ resistor. Before each session instrumental baselines were measured and amplifier gains intercalibrated. Measurements consisted of 80 s of solution uptake to allow the ion beams to stabilise. Sample and standard measurements were preceded by 90 s of washing with 0.4 M HCl – 0.05 M HF, followed an on-peak baseline measurement of reagent blank, 0.2 M HCl, for 20 cycles of 4.194 s integration time. Individual sample and standard measurements consisted of 80 cycles each, with 4.194 s integration time. Each sample was preceded and followed by a measurement of the double-spiked (with a double spike proportion similar to samples) standard CRM-145. Samples and standard were measured at varying concentrations, generally between 100 to 300 ng g⁻¹, correlating to U consumption between ~ 30 to 80 ng per measurement. Procedural blanks were <30 pg U, an insignificant amount compared to amount of U consumed per measurement. Ion beam intensities were corrected for low mass tailings of ion beams and high mass plus hydride tailings of ion beams following Andersen et al. (2015). Each solution was corrected for solution blank and intensities re-calculated.

The measured double spike isotope ratio of ²³³U/²³⁶U (Richter et al., 2008) was used with the exponential mass fractionation law to correct for mass fractionation of isotope ratios in samples and bracketing standards. Ratios were also corrected for the minute ²³⁸U, ²³⁵U, and ²³⁴U contributions from the IRM-3636 double spike (Condon et al., 2010; Hiess et al., 2012). Uranium

isotope ratios for $^{238}\text{U}/^{235}\text{U}$ and $^{234}\text{U}/^{238}\text{U}$ are reported in δ notation with $\delta^{238}\text{U} = [(^{238}\text{U}/^{235}\text{U}_{\text{Sample}} / ^{238}\text{U}/^{235}\text{U}_{\text{CRM-145}}) - 1]$ and $\delta^{234}\text{U} = [(^{234}\text{U}/^{238}\text{U}_{\text{Sample}} / (^{234}\text{U}/^{238}\text{U}_{\text{CRM-145}} / (1-0.0386))) - 1]$. By normalising sample measurements to the average of bracketing CRM-145 analyses, this removes second order non-exponential mass bias effects from the analyses. Note that $\delta^{234}\text{U}$ values are reported relative to secular equilibrium, where the CRM-145 standard has a $\delta^{234}\text{U}$ of -38.6 ‰ relative to secular equilibrium (Cheng et al., 2013).

Long term external reproducibility at various measured U intensities has been estimated using aliquots of the well characterised reference material BHVO-2 measured during different analytical sessions. The external reproducibility of $\delta^{238}\text{U}$ and $\delta^{234}\text{U}$ for BHVO-2 at various intensities (e.g., $^{238}\text{U} = 200$ to 1000 pA) ranges from ± 0.09 to 0.03 ‰ , 2sd, and ± 4 to 0.9 ‰ , 2sd, respectively. The external reproducibility of unknown samples has been determined from the long-term external reproducibility of BHVO-2 measured at various intensities. As samples were measured at varying intensities ($\sim ^{238}\text{U} = 200$ to 1000 pA) depending on the U concentration, BHVO-2 was also ran at varying intensities. Repeat measurements of BHVO-2 were then used to construct error curves using the two standard deviations of measurements in ranges of intensities. A power law was fit to the data for $\delta^{238}\text{U}$ and $\delta^{234}\text{U}$ at the different intensities and used to approximate errors for unknown samples. This relationship was then used for samples of a given concentration, that corresponds to a given intensity, from which an approximate 2sd could be calculated and an external 2se calculated based on the number of repeats (Fig. S4).

Uranium isotopic measurements of international reference materials analysed (BHVO-2, BCR-2, BIR, uraninite, and CZ-1) agree well with values reported by other studies (Table S3). We also report data for a set of in-house reference materials (LP-45d, GUG-11, and IT-3a) that agree well with previous data, and report data on international reference material W-2A, such that it can be used for comparison in further studies. Full list of reference material data is provided in table S3.

Collected Mo fractions from the TRU resin U chemistry (40 ml of sample load and first 10 ml of 1.5 M HNO_3 wash) were dried and dissolved for chemistry using Eichrom AG 1-X8 100 – 200 mesh anionic resin, following Willbold et al. (2016). Samples were dissolved in 22.5 ml 3 M HCl and 1.25 ml 6 M HCl ready for column chemistry using 2 ml of Eichrom AG 1-X8 100 – 200 mesh

anionic resin in Bio-Rad Poly-Prep columns. At least an hour before samples were loaded onto columns, 1.25 ml of 1 M Ascorbic acid was added to samples and allowed to react to reduce Fe^{3+} to Fe^{2+} which is identified by a colour change of samples from yellow to green/colourless. Matrix was eluted using 6 ml 3 M HCl, 26 ml 0.5 M HCl- 0.5 % H_2O_2 , 20 ml 1 M HF and 6 ml milli-Q water, before collection of Mo in 24 ml of 1 M HCl. Collected Mo fractions were dried and fluxed in a 1 ml 50:50 15.6 M HNO_3 : 30 % Romil SpA H_2O_2 mixture to eliminate any organic material that may have leached off resin into samples. Samples were dried and re-dissolved in the requisite amount of 0.4 M HNO_3 – 0.4 M HF for a Mo concentration of 200 ng g^{-1} for isotopic analysis.

Processing samples through the U chemistry first has the potential to increase the Mo procedural blank, however procedural blanks for Mo that had been processed through the TRU resins and AG 1-X8 columns were ~ 340 and 380 pg (2 separate procedural blanks); on the same order of magnitude as other studies (Willbold et al., 2016; Chen et al., 2022) and negligible compared to amount of Mo measured (~ 30 ng).

Molybdenum isotopic compositions were measured on a ThermoFinnigan Neptune MC-ICP-MS (serial no. 1020) at the Bristol Isotope group in low mass resolution ($M/\Delta M \sim 1600$, 5 to 95 % peak height definition). Samples were introduced to the plasma using a ~ 40 ul min^{-1} micro-concentric PFA nebuliser connected to a Cetac Aridus (1st generation) desolvating system. Nitrogen and argon flow rates were tuned at the start of each session for optimal sensitivity and stability. A standard sample cone plus H-skimmer cone setup was used. Masses 91 (^{91}Zr), 92 (^{92}Mo), 95 (^{95}Mo), 96 (^{96}Mo), 97 (^{97}Mo), 98 (^{98}Mo), 99 (^{99}Ru), 100 (^{100}Mo), and 101 (^{101}Ru) were collected in faraday cups L4 to H4 respectively. All cups would ideally be connected to an amplifier with a $10^{11} \Omega$ resistor, however due to the limited number of $10^{11} \Omega$ resistors available on the Neptune, ^{91}Zr , ^{92}Mo , and ^{101}Ru were connected to $10^{10} \Omega$ resistors. This should not be an issue as ^{91}Zr and ^{101}Ru are interferences and removed in chemistry and ^{92}Mo is not used in the double spike inversion for the calculation of $^{98}\text{Mo}/^{95}\text{Mo}$. Before each session instrumental baselines were measured and amplifier gains intercalibrated. Measurements consisted of 80 s of solution uptake to allow the ion beams to stabilise. Sample and standard measurements were preceded by 90 s of washing with 0.4 M HNO_3 – 0.4 M HF, followed an on-peak baseline measurement of reagent, 0.4 M HNO_3 – 0.4 M HF, blank for 30 cycles of 4.194 s integration time.

Individual sample and standard measurements consisted of 30 cycles of 4.194 s integration time, consuming ~ 30 ng Mo per measurement for solutions measured at 200 ng g^{-1} . Each sample was preceded and followed by a measurement of the double-spiked (with a double spike proportion similar to samples) standard NIST SRM3134. Each solution was corrected for solution blank and intensities re-calculated.

Measurements were internally normalised using a double spike inversion using ^{95}Mo , ^{97}Mo , ^{98}Mo , and ^{100}Mo , and $^{98}\text{Mo}/^{95}\text{Mo}$ ratios calculated. Samples were externally normalised to the bracketing standard and $\delta^{98/95}\text{Mo}$ calculated ($\delta^{98/95}\text{Mo} = [(^{98}\text{Mo}/^{95}\text{Mo}_{\text{Sample}} / ^{98}\text{Mo}/^{95}\text{Mo}_{\text{NISTSRM3134}}) - 1]$). Ruthenium has interferences with ^{98}Mo (^{98}Ru) and ^{100}Mo (^{100}Ru). Therefore, ^{99}Ru and ^{101}Ru were monitored to allow for corrections to be applied to ^{98}Mo and ^{100}Mo . Ruthenium doping experiments (Chen et al., 2019) show that corrections using ^{99}Ru can accurately correct Mo data. However, there is the potential for overcorrection due to species such as $^{64}\text{Zn}^{35}\text{Cl}$ and $^{40}\text{Ar}_2^{19}\text{F}$ giving signals at mass 99 (Chen et al., 2019). Therefore, ^{101}Ru is also monitored and can be used for correction. Data was corrected using both ^{99}Ru and ^{101}Ru , and when compared, both methods give the same answer within uncertainty. If the total Ru correction was ever over 0.1 ‰ in $\delta^{98/95}\text{Mo}$ the datum was rejected (no data in this study was rejected).

We take a homoscedastic approach to determine our external reproducibility, pooled 2sd, on any single stable Mo isotopic measurement, i.e., one standard-sample-standard measurement (Table S4). Using this approach, we define an external reproducibility of $\delta^{98/95}\text{Mo} \pm 0.05 \text{ ‰}$, 2sd, for a single measurement in a given run. This pooled 2sd is then used to calculate the standard error for a given sample given the number, n , of repeat measurements, typically 4 to 6 for unknown samples. This is identical to the 2sd, $\pm 0.05 \text{ ‰}$, of 35 repeats of W-2A measured over 4 digestions across 4 measuring sessions, and is similar to that reported in Chen et al. (2022) and Hin et al. (2022). Molybdenum isotopic measurements of international reference materials analysed (BHVO-2, BCR-2, and W-2A) agree well with literature data (Table S4), as well as our data for other internal standards (CPI and GUG-11). A full list of data for reference materials is provided in table S5.

Section 3:

Supplementary figures and tables

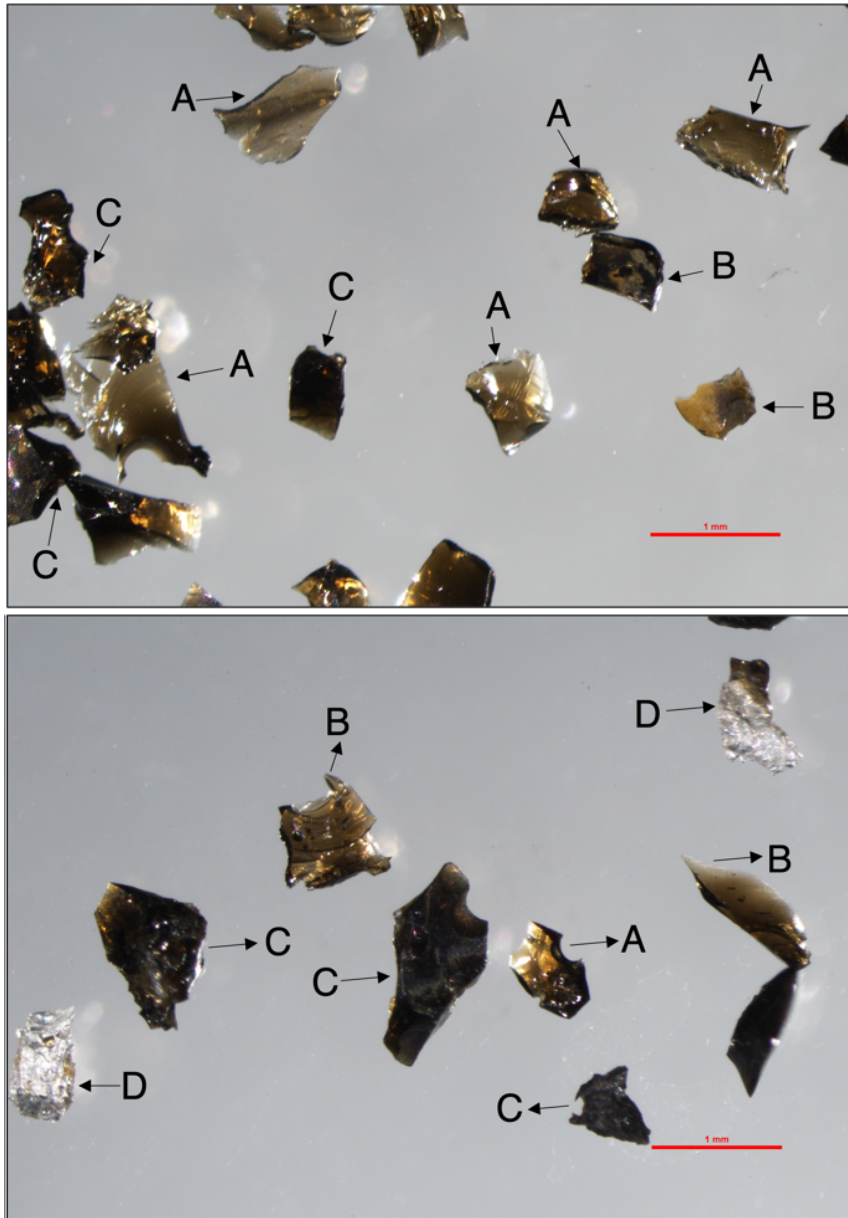


Fig. S1. Example of different qualities of MORB glass picked for sample JC24-80-23. Red scale bar is 1 mm. The letter assigned denotes the quality of glass described in the supplementary text.

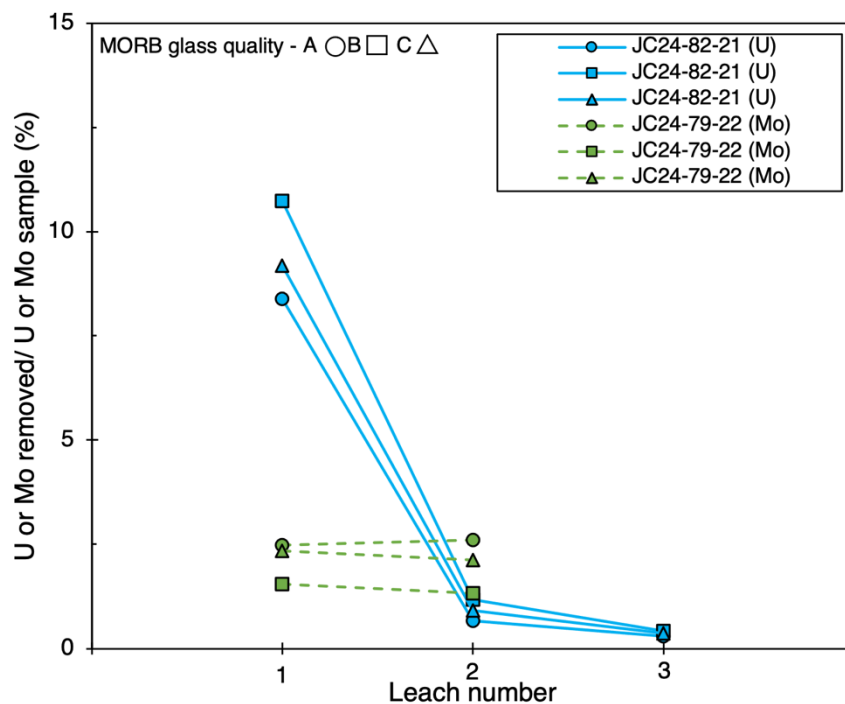


Fig. S2. Percentage of total U (blue) and Mo (green) lost in successive leaches of MORB glass for different glass qualities picked.

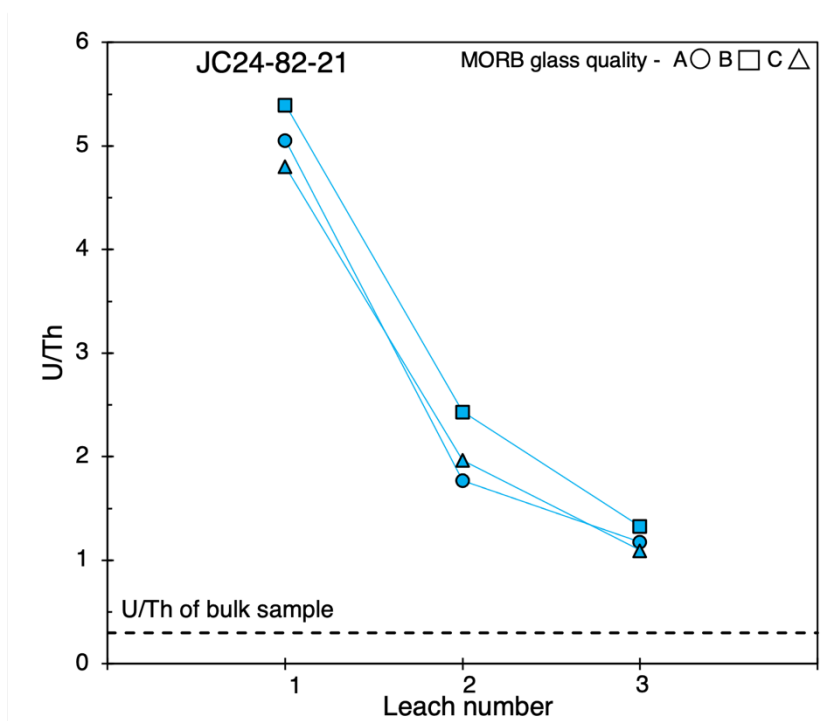


Fig. S3. U/Th ratios in successive leaches of MORB glass for sample JC24-82-21.

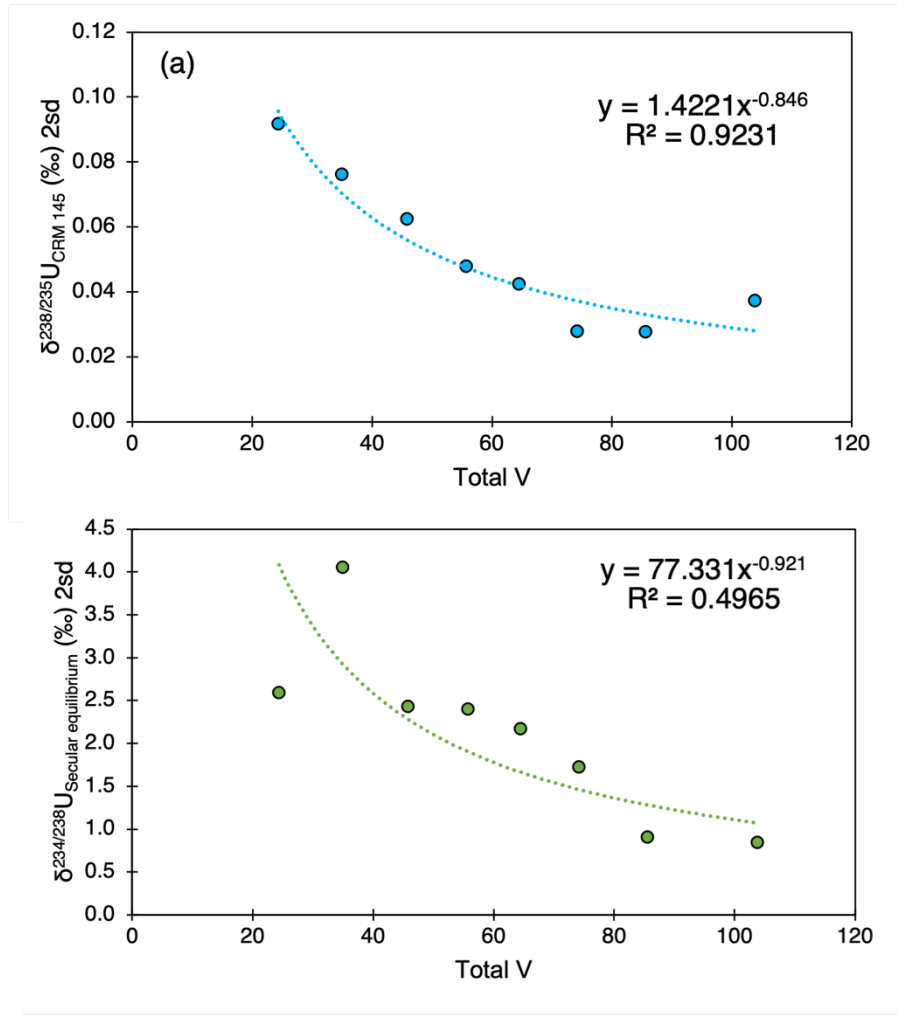
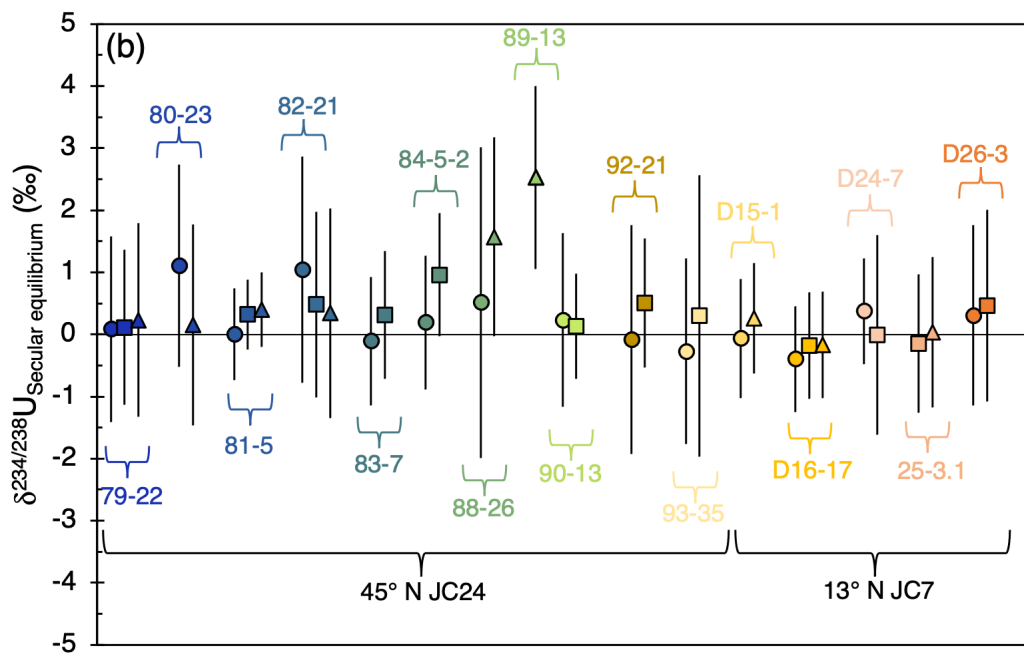
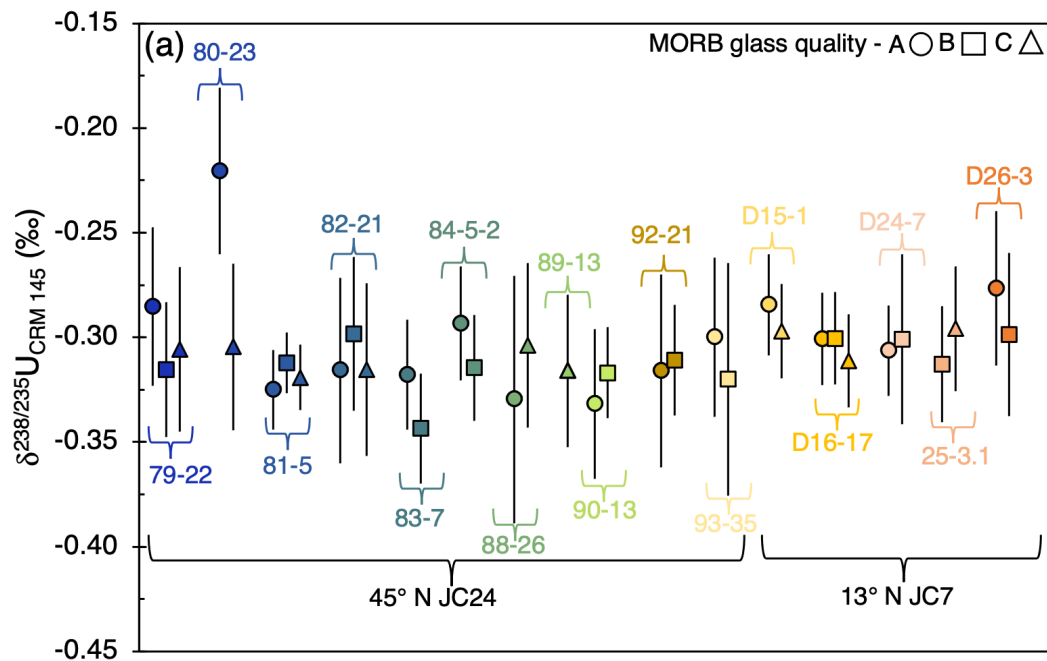


Fig. S4. Error curves for BHVO-2 constructed using the external 2sd of repeat measurements of BHVO-2 at various intensity brackets, $\geq 20 < 30$ V, $\geq 30 < 40$ V, $\geq 40 < 50$ V, $\geq 50 < 60$ V, $\geq 60 < 70$ V, $\geq 70 < 80$ V, $\geq 80 < 90$ V and ≥ 90 V. A power law relationship is fit through the external 2sd. The relationship defined by the power law is then applied to approximate errors for unknown samples. (a) Error curve for $\delta^{238}U$ measurements, (b) Error curve for $\delta^{234}U$ measurements.



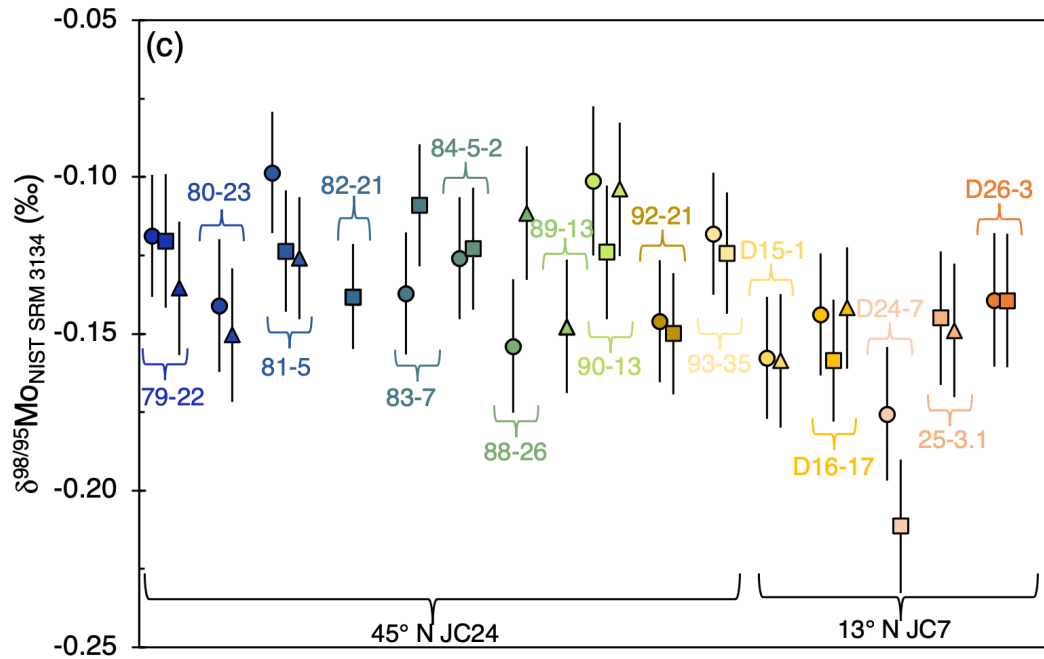


Fig. S5. Isotopic composition of different qualities of MORB glass samples, (a) $\delta^{238}\text{U}$ (b) $\delta^{234}\text{U}$ and (c) $\delta^{98/95}\text{Mo}$. Error bars are 2se.

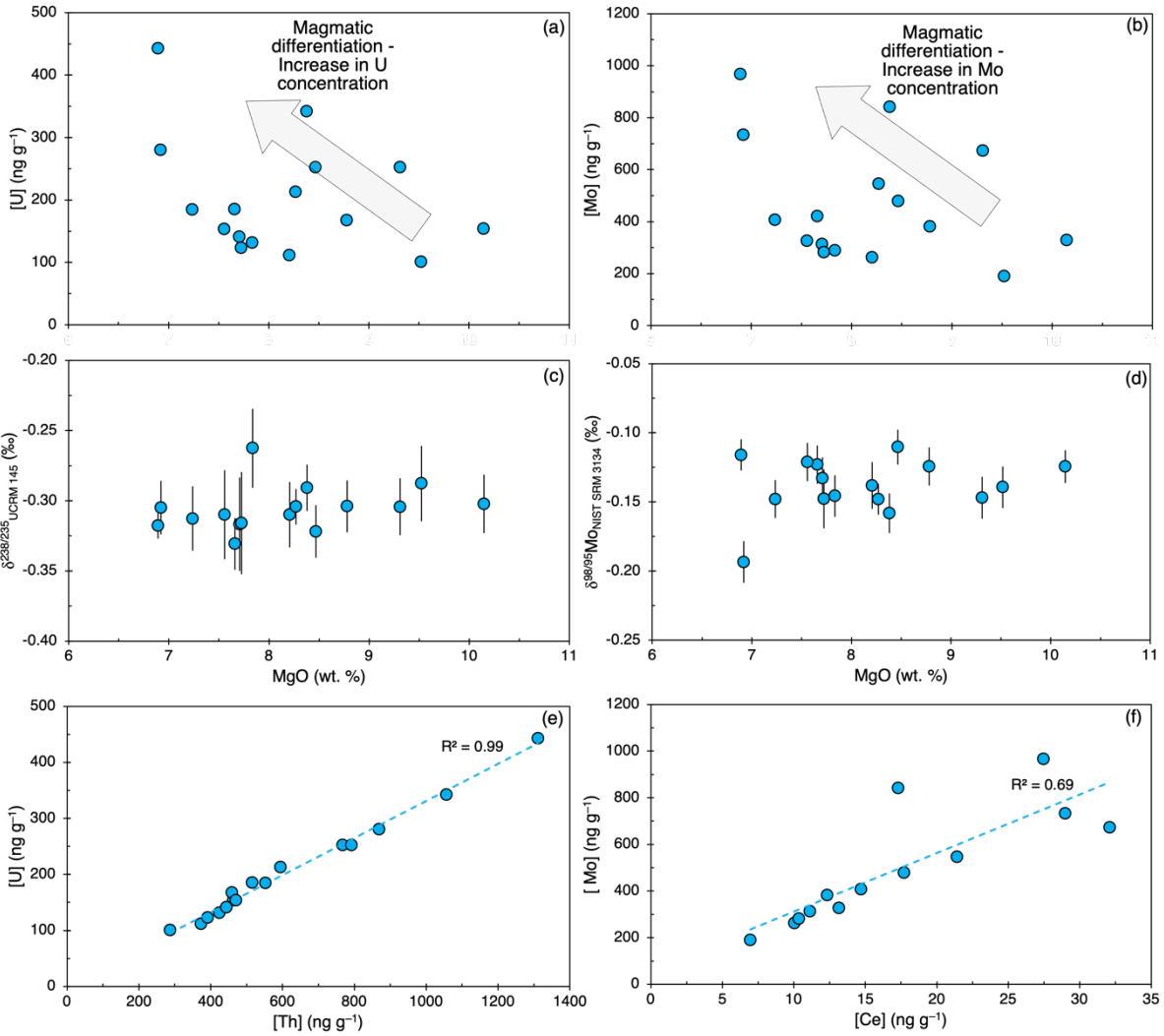


Fig. S6. Variations of E-MORB samples in this study of (a) U concentration, (b) Mo concentration (c) $\delta^{238}\text{U}$ and (d) $\delta^{98/95}\text{Mo}$ with MgO as a tracer of magmatic differentiation. Linear variation in (e) the U and Th concentration and (f) Mo and Ce concentration of E-MORB samples, trend line is shown as a dashed line with its associated R^2 value.

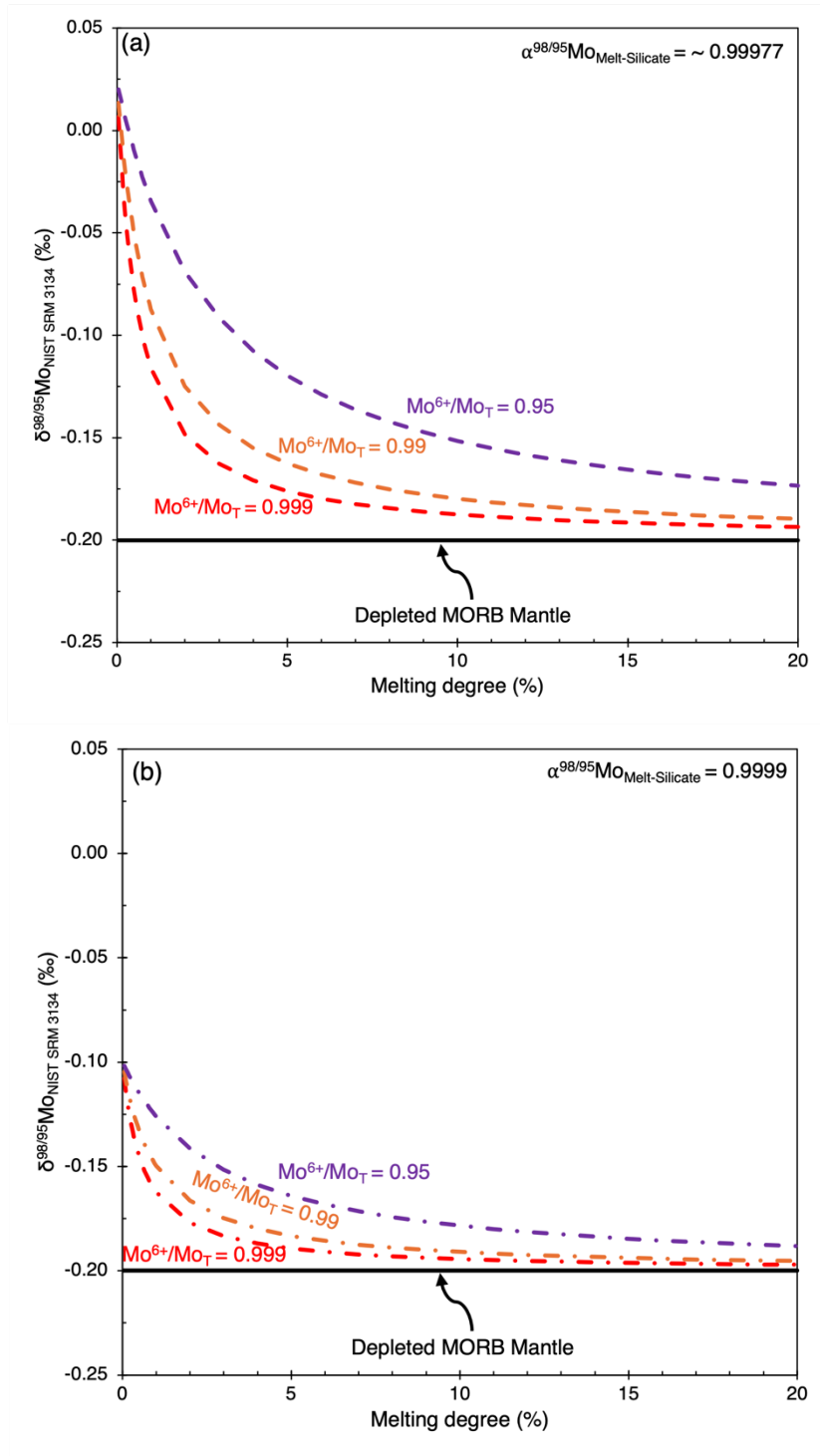


Fig. S7. Non-modal batch melting modelling of Mo isotope composition of melt as a function of melting degree. Model calculations follow McCoy-West et al. (2019) and Chen et al. (2022), parameters used are given in table S8. Compositions are calculated at different mantle $f\text{O}_2$ ($\text{Mo}^{6+}/\text{Mo}_T = 0.999$ to 0.95) and start from DMM compositions of $\delta^{98/95}\text{Mo} = -0.2 \text{ ‰}$ with $\alpha^{98/95}\text{Mo}_{\text{Melt-Silicate}}$ of (a) ~ 0.99977 and (b) 0.9999 .

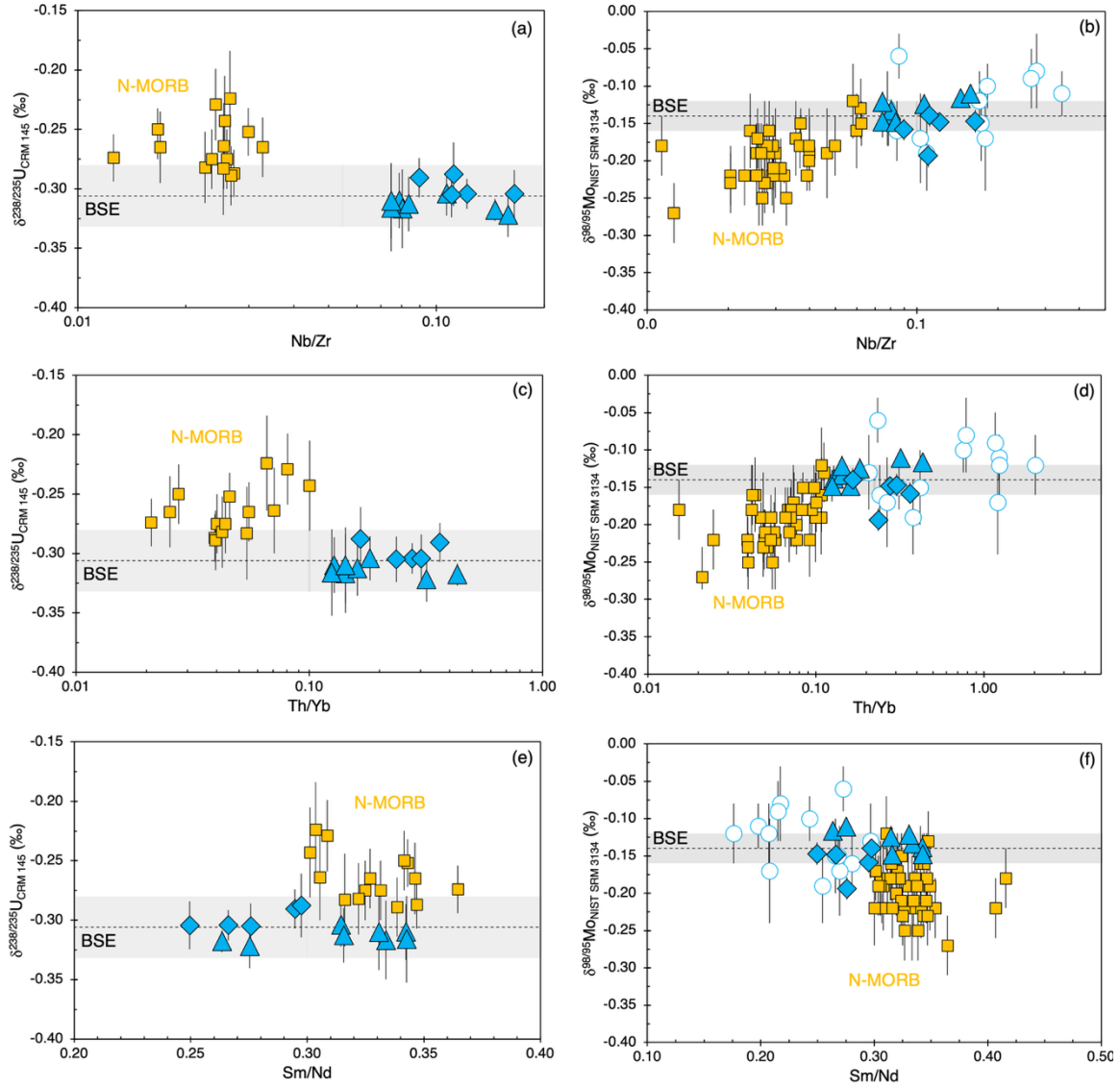


Fig. S8. (a, c, e) $\delta^{238}\text{U}$ and (b, d, f) $\delta^{98/95}\text{Mo}$ versus (a, b) Nb/Zr, (c, d) Th/Yb, (Sm/Nd) of MORB samples. Enriched-MORB from this study are shown as filled blue symbols and grouped into samples from 45°N (triangles) and 13°N (diamonds). Average N-MORB (yellow squares) concentrations are from Gale et al. (2013). Isotopic data for BSE and N-MORB are from the same sources as in figure 2, and literature E-MORB (hollow circles) are from Bezard et al. (2016), Chen et al. (2022) and Hin et al. (2022). Error bars are $\pm 2\text{se}$. Grey shaded regions represents isotopic compositions of BSE ($\pm 2\text{se}$).

Region	Sample	Latitude (°N)	Longitude (°W)	Depth (m)	Age (Ma)	
MAR 45 °N	JC24	79-22	45.49	27.86	2568	1
		80-23	45.44	27.88	2651	2.5
		81-5	45.71	27.78	3457	3
		81-21	45.62	27.85	3062	2.5
		83-7	45.55	27.89	3326	1.5
		84-5-2	45.55	27.88	3088	1
		88-26	45.39	27.88	3048	1.5
		89-13	45.59	27.81	3511	2
		90-13	45.60	27.84	2949	1.5
		92-21	45.48	27.89	3032	2
		93-35	45.48	27.87	2632	1.8
MAR 13 °N	JC7	D15-1	13.07	44.09	4496	0.5 – 1
		D16-17	13.03	44.84	4820	0.5 – 1
		D24-7	13.35	44.90	3011	0.5 – 1
		25-3.1	13.40	44.89	3857	0.5 – 1
		D26-3	13.66	44.97	3496	0.5 – 1

Table S1. E-MORB samples used in this study from the Northern Mid-Atlantic ridge, data for 13 °N is from Wilson et al. (2013).

Sample	BHVO-2	W-2A
Th (ng g ⁻¹)	1129	2112
Th 2sd	165	401
Th 2se	14	51
U (ng g ⁻¹)	383	469
U 2sd	57	85
U 2se	5	11
Th/U	2.9	4.5
(Th, U) N	147	63
Mo (ng g ⁻¹)	3645	400
Mo 2sd	734	104
Mo 2se	88	13
(Mo) N	69	63
Reference Th (ng g ⁻¹)	1114	2179
Reference U (ng g ⁻¹)	386	490
Reference Th/U	2.9	4.4
Reference Mo	4070	410

Table S2. List of reference materials used to check reproducibility and precision of measurements of Th, U, and Mo concentrations measured on an ICP-MS Element2. Reference values are from the USGS data sheets.

Sample	$\delta^{238}\text{U}$ (‰)	2sd	$\delta^{234}\text{U}$ (‰)	2sd	[U] (ng g ⁻¹)*	N.M	N.S
BHVO-2	-0.306	0.044	-0.1	1.8	419	145	25
	<i>-0.314</i>	<i>0.020</i>	<i>0.9</i>	<i>2.4</i>	<i>386</i>	<i>16</i>	<i>8</i>
BCR-2	-0.255	0.036	0.6	1.4	1687	27	4
	<i>-0.297</i>	<i>0.020</i>	<i>1.1</i>	<i>1.0</i>	<i>1671</i>	<i>1</i>	<i>1</i>
BIR	-0.277	0.189	-5.1	8.6	8	6	3
	<i>-0.285</i>	<i>0.020</i>	<i>-0.6</i>	<i>1.0</i>	<i>8</i>	<i>1</i>	<i>1</i>
CZ-1	-0.048	0.045	-0.2	1.8	7995	30	3
	<i>-0.053</i>	<i>0.030</i>	<i>0.1</i>	<i>2.7</i>		<i>15</i>	<i>2</i>
GUG-11	-0.460	0.050	0.3	2.0	185	10	2
	<i>-0.419</i>	<i>0.030</i>	<i>-0.4</i>	<i>2.0</i>	<i>143</i>	<i>1</i>	<i>1</i>
IT-3a	-0.289	0.063	0.1	2.6	70	26	10
	<i>-0.296</i>	<i>0.020</i>	<i>-0.3</i>	<i>1.7</i>	<i>62</i>	<i>3</i>	<i>1</i>
LP-45d	-0.319	0.049	-0.2	2.0	2356	83	3
	<i>-0.300</i>	<i>0.020</i>	<i>-0.3</i>	<i>4.5</i>	<i>2119</i>	<i>5</i>	<i>2</i>
Uraninite	-0.548	0.053	-1.5	2.1	11985	51	3
W-2A	-0.291	0.036	2.0	1.4	497	37	7

Table S3. List of reference materials used to check reproducibility and precision during analytical sessions. Data in blue and italics are from Andersen et al. (2015). * Concentrations of U determined from isotope dilution. N.M is the number of individual measurements and N.S is the number of individual samples dissolved and processed through column chromatography.

Sample	2sd	N	Variance $\times (N-1)$
W-2a	0.05	35	0.0184
GUG-11	0.05	19	0.0108
CPI	0.04	56	0.0212
BHVO-2	0.05	20	0.0140
BCR-2	0.05	8	0.0038
JC24-80-23-AB	0.03	5	0.0010
JC24-80-23-C	0.08	5	0.0070
JC24-88-26-C	0.03	5	0.0008
JC24-88-26-AB	0.06	5	0.0032
JC24-89-13	0.08	5	0.0070
JC7-25-3.1-C	0.04	5	0.0019
JC7-25-3.1-B	0.02	5	0.0004
JC24-83-7-A	0.05	6	0.0035
JC24-83-7-B	0.02	6	0.0007
JC24-84-5-2-A	0.03	6	0.0015
JC24-84-5-2-B	0.04	6	0.0022
JC24-92-21-A	0.05	6	0.0036
JC24-92-21-B	0.07	6	0.0057
JC24-93-35-A	0.05	6	0.0033
JC24-93-35-B	0.03	6	0.0012
JC7-D15-1-A	0.06	6	0.0048
JC7-D15-1-C	0.04	5	0.0012
JC7-D24-7-A	0.01	5	0.0001
JC7-D24-7-B	0.06	5	0.0033
JC7-D26-3-A	0.02	5	0.0004
JC7-D26-3-B	0.03	5	0.0012
JC7-D16-17-A	0.05	6	0.0034
JC7-D16-17-B	0.06	6	0.0052
JC7-D16-17-C	0.06	6	0.0050
JC24-81-5-A	0.06	6	0.0044
JC24-81-5-B	0.06	6	0.0048
JC24-81-5-C	0.06	6	0.0044
JC24-79-22-A	0.04	6	0.0023

JC24-79-22-B	0.04	5	0.0018
JC24-79-22-C	0.02	5	0.0003
JC24-90-13-A	0.05	4	0.0018
JC24-90-13-B	0.04	5	0.0016
JC24-90-13-C	0.04	5	0.0012
JC24-82-21-B	0.04	8	0.0035
Sum		326	0.16
Pooled variance	0.0006		
Pooled 2sd	0.05		

Table S4. Homoscedastic approach for calculating external uncertainty on Mo isotopic compositions. Variance is calculated as $\text{Variance} = 2\text{sd}^2/4$ and pooled variance as the sum of variance $\times (N-1) / \text{sum of } N-1$. Pooled 2sd is calculated as $\text{pooled 2sd} = 2 \times \sqrt{\text{Pooled variance}}$.

1791
1792
1793
1794
1795
1796
1797
1798
1799
1800
1801
1802
1803
1804
1805
1806
1807
1808
1809
1810
1811
1812
1813
1814
1815
1816

Sample	$\delta^{98/95}\text{Mo}$ (‰)	2sd	2se	[Mo] ppb*	N.M	N.S
CPI	-0.27 <i>-0.23</i>	0.05 <i>0.04</i>			56 <i>42</i>	
BHVO-2	-0.06 <i>-0.08</i>	0.05 <i>0.04</i>		4207 <i>3570</i>	20 <i>6</i>	3
W-2A	-0.05 <i>-0.05</i>	0.05 <i>0.05</i>		417 <i>460</i>	35 <i>9</i>	4
GUG11	0.07 <i>0.049</i>	0.05	<i>0.016</i>	946 <i>1003</i>	19	1
BCR-2	0.00 <i>-0.03</i>	0.05 <i>0.04</i>		259873 <i>236000</i>	8 <i>3</i>	1

Table S5. List of reference materials used to check reproducibility and precision during analytical sessions. Data in blue and italics are from Freymuth et al. (2015): GUG-11, Willbold et al. (2016): CPI, Liang et al. (2017): BCR-2, and Chen et al. (2022): BHVO-2 and W-2A. * Concentrations of Mo determined from double spiking. N.M is the number of individual measurements and N.S is the number of individual samples dissolved and processed through column chromatography.

Sample	U (ng g ⁻¹)	Th/U	$\delta^{238}\text{U}$ (‰)	2se	$\delta^{234}\text{U}$ (‰)	2se	N	Mo (ng g ⁻¹)	Ce/Mo	$\delta^{98/95}\text{Mo}$ (‰)	2se	N	K ₂ O/TiO ₂	(La/Sm) _N
45° N JC24	79-22	154	3.01	-0.302	0.021	0.1	0.8	3	328	-0.12	0.01	16	0.11	
	80-23	132	3.23	-0.263	0.028	0.6	1.1	4	289	-0.15	0.02	10	0.11	
	81-5	443	2.96	-0.318	0.009	0.3	0.4	12	967	28.4	-0.12	0.01	18	0.30
	82-21	111	3.35	-0.310	0.023	0.6	1.0	6	262	38.3	-0.14	0.02	8	0.13
	83-7	185	2.79	-0.331	0.019	0.1	0.7	4	420	-0.12	0.01	12	0.16	1.87
	84-5-2	167	2.74	-0.304	0.019	0.6	0.7	4	382	32.3	-0.12	0.01	12	0.17
	88-26	141	3.15	-0.317	0.033	1.0	1.4	4	313	35.6	-0.13	0.02	10	0.12
	89-13	123	3.18	-0.316	0.036	2.5	1.5	2	282	36.8	-0.15	0.02	5	0.11
	90-13	252	3.04	-0.322	0.019	0.2	0.7	3	479	37.0	-0.11	0.01	14	0.27
	92-21	185	2.99	-0.313	0.023	0.3	0.9	3	407	36.1	-0.15	0.01	12	0.14
13° N JC7	93-35	153	3.06	-0.310	0.032	0.0	1.3	2	327	40.3	-0.12	0.01	12	0.12
	D15-1	342	3.09	-0.291	0.016	0.1	0.7	6	842	20.6	-0.16	0.01	11	0.35
	D16-17	213	2.80	-0.304	0.013	-0.2	0.5	6	546	39.2	-0.15	0.01	18	0.19
	D24-7	280	3.10	-0.305	0.019	0.3	0.8	4	733	39.5	-0.19	0.02	10	0.37
	25-3.1	252	3.14	-0.304	0.020	-0.1	0.8	6	672	47.8	-0.15	0.02	10	0.14
Atl. E- MORB	D26-3	101	2.86	-0.288	0.027	0.4	1.1	2	189	36.7	-0.14	0.02	10	0.22
				-0.307	0.008	0.3	0.3			-0.14	0.01			

Table S6. U and Mo concentration and isotopic data for E-MORB samples analysed in this work (mean compositions from multiple qualities of glass for each sample), along with select element ratios. Error is the 2se and N refers to the total number of repeat measurements. For the overall Atlantic E-MORB average, isotopic compositions are calculated as concentrated weighted averages, and the error calculated as the 2sd over the square root of total number of samples measured.

Sample		Mass picked (mg)	U (ng g ⁻¹)	δ ²³⁸ U (‰)	2se	δ ²³⁴ U (‰)	2se	N	Mo (ng g ⁻¹)	δ ^{98/95} Mo (‰)	2se	N
45° N JC24	79-22-A	544	154	-0.285	0.038	0.1	1.5	1	329	-0.12	0.02	6
	79-22-B	1056	154	-0.315	0.032	0.1	1.3	1	330	-0.12	0.02	5
	79-22-C	664	153	-0.306	0.039	0.2	1.6	1	325	-0.14	0.02	5
	79-22		154	-0.302	0.021	0.1	0.8	3	328	-0.12	0.01	16
	80-23-AB	814	133	-0.221	0.040	1.1	1.6	2	292	-0.14	0.02	5
	80-23-C	788	130	-0.305	0.040	0.2	1.6	2	286	-0.15	0.02	5
	80-23		132	-0.263	0.028	0.6	1.1	4	289	-0.15	0.02	10
	81-5-A	760	449	-0.325	0.019	0.0	0.7	3	976	-0.10	0.02	6
	81-5-B	1182	443	-0.312	0.014	0.3	0.6	5	964	-0.12	0.02	6
	81-5-C	1009	437	-0.319	0.016	0.4	0.6	4	960	-0.13	0.02	6
	81-5		443	-0.318	0.009	0.3	0.4	12	967	-0.12	0.01	18
	82-21-A	1042	112	-0.316	0.044	1.0	1.8	2				
	82-21-B	1154	111	-0.298	0.037	0.5	1.5	2	262	-0.14	0.02	8
	82-21-C	1055	111	-0.315	0.041	0.3	1.7	2				
	82-21		111	-0.310	0.023	0.6	1.0	6	262	-0.14	0.02	8
	83-7-A	991	185	-0.318	0.026	-0.1	1.0	2	421	-0.14	0.02	6
	83-7-B	1058	185	-0.344	0.026	0.3	1.0	2	420	-0.11	0.02	6
	83-7		185	-0.331	0.019	0.1	0.7	4	420	-0.12	0.01	12
	84-5-2-A	1030	168	-0.293	0.027	0.2	1.1	2	385	-0.13	0.02	6
	84-5-2-B	1069	166	-0.314	0.025	1.0	1.0	2	379	-0.12	0.02	6
	84-5-2		167	-0.304	0.019	0.6	0.7	4	382	-0.12	0.01	12
	88-26-C	1090	140	-0.304	0.039	1.6	1.6	2	315	-0.11	0.02	5
	88-26-AB	720	143	-0.330	0.059	0.5	2.5	2	310	-0.15	0.02	5
	88-26		141	-0.317	0.033	1.0	1.4	4	313	-0.13	0.02	10
	89-13	990	123	-0.316	0.036	2.5	1.5	2	282	-0.15	0.02	5
	90-13-A	519	253	-0.332	0.036	0.2	1.4	1	480	-0.10	0.02	4
	90-13-B	1054	252	-0.317	0.022	0.1	0.8	2	480	-0.12	0.02	5
	90-13-C	905							477	-0.10	0.02	5
	90-13		252	-0.322	0.019	0.2	0.7	3	479	-0.11	0.01	14
	92-21-A	524	184	-0.316	0.046	-0.1	1.8	1	407	-0.15	0.02	6
	92-21-B	1041	185	-0.311	0.026	0.5	1.0	2	407	-0.15	0.02	6
	92-21		185	-0.313	0.023	0.3	0.9	3	407	-0.15	0.01	12
	93-35-A	848	148	-0.300	0.038	-0.3	1.5	1	315	-0.12	0.02	6
	93-35-B	501	159	-0.320	0.056	0.3	2.3	1	338	-0.12	0.02	6
	93-35		153	-0.310	0.032	0.0	1.3	2	327	-0.12	0.01	12
13° N JC7	D15-1-A	828	343	-0.284	0.024	-0.1	1.0	3	845	-0.16	0.02	6
	D15-1-C	933	340	-0.297	0.023	0.3	0.9	3	838	-0.16	0.02	5
	D15-1		342	-0.291	0.016	0.1	0.7	6	842	-0.16	0.01	11
	D16-17-A	992	214	-0.301	0.022	-0.4	0.9	2	546	-0.14	0.02	6
	D16-17-B	1182	212	-0.300	0.022	-0.2	0.9	2	546	-0.16	0.02	6
	D16-17-C	1131	212	-0.311	0.022	-0.2	0.9	2	545	-0.14	0.02	6
	D16-17		213	-0.304	0.013	-0.2	0.5	6	546	-0.15	0.01	18
	D24-7-A	1090	282	-0.306	0.022	0.4	0.9	3	729	-0.18	0.02	5
	D24-7-B	492	275	-0.301	0.041	0.0	1.6	1	737	-0.21	0.02	5
	D24-7		280	-0.305	0.019	0.3	0.8	4	733	-0.19	0.02	10
	25-3.1-C	917	252	-0.296	0.030	0.0	1.2	3	675	-0.15	0.02	5
	25-3.1-B	822	253	-0.313	0.028	-0.2	1.1	3	670	-0.14	0.02	5
	25-3.1		252	-0.304	0.020	-0.1	0.8	6	672	-0.15	0.02	10
	D26-3-A	1031	101	-0.277	0.037	0.3	1.5	1	201	-0.14	0.02	5
	D26-3-B	1019	100	-0.299	0.039	0.5	1.5	1	178	-0.14	0.02	5
	D26-3		101	-0.288	0.027	0.4	1.1	2	189	-0.14	0.02	10

Table S7. Full table of amounts of MORB glass picked, U and Mo concentrations and isotopic compositions of MORB glass samples measured in this work split into each quality of MORB glass measured, mean compositions are shown in bold. For mean compositions the average is calculated as the average over all individual measurements.

	Pb (ug g ⁻¹)	Ce (ug g ⁻¹)	Ce/Pb	²⁰⁷ Pb/ ²⁰⁴ Pb
Igneous oceanic crust	0.48 ^a	11.95 ^a	24.9	15.53 ^b
Recycled oceanic crust	0.0912 ^a	5.8555 ^a	64.21	15.53 ^b
Mobility (%)	81 ^a	51 ^a		
GLOSS-II	21.2 ^c	57.6 ^c	2.7	15.694 ^c
GLOSS-II melt	18.444 ^a	44.352 ^a	2.4	15.694 ^c
Mobility Sediment-Melt (%)	13 ^a	23 ^a		
DMM	0.0232 ^d	0.772 ^d	33.3	15.515 ^e

1873 Table S8. Compositions used in the mixing models shown in figure 5. a - Stracke et
1874 al. (2003). b – 801C average from Hauff et al. (2003). c – Plank (2014). d – Salters
1875 and Stracke (2004). e – Gale et al. (2013). The composition of recycled oceanic crust
1876 and GLOSS-II melt have been calculated using the element mobility % given in
1877 Stracke et al. (2003).

Phase	Olivine	Orthopyroxene	Clinopyroxene	Garnet
D _{La}	0.0005	0.004	0.015	0.0007
D _{Sm}	0.0011	0.02	0.1509	0.23
D _{Mo}	0.013	0.026	0.0053	0.017*
D _{Mo} ⁴⁺	0.5	0.7	0.3	
D _{Mo} ⁶⁺	0.006	0.009	0.001	
K ⁻¹	0.0000074	0.000012	0.0000015	
Modal %	0.52	0.22	0.16	0.1
Melt mode %	0.08	-0.19	0.81	0.3
DMM	Concentration (ug g ⁻¹)	Isotopic composition (‰)		
La	0.234			
Sm	0.270			
Mo	0.025	-0.2 / -0.185		
Force constant	Mineral	Melt		
Mo	650	1041		

1878 Table S9. Model parameters for non-modal batch melting calculation and Mo isotopic
1879 fractionation. Partition coefficients for La and Sm are from Salters and Stracke (2004). Partition
1880 coefficients for Mo and K⁻¹ are from Leitzke et al. (2017). Partition coefficient for Mo in garnet

is assumed to be \approx to Ce and is taken from Salters and Stracke (2004). Modal % and Melt modes % are from Walter (1998). Depleted MORB Mantle (DMM) compositions are from Salters and Stracke (2004) and isotopic compositions are from Hin et al. (2022). Force constants for Mo in mineral and melt are from McCoy-West et al. (2019). Non-modal batch melting models and Mo isotopic fractionation models follow McCoy-West et al. (2019) and Chen et al. (2022).

References

- Andersen, M. B., S. Romaniello, D. Vance, S. H. Little, R. Herdman, and T. W. Lyons, 2014, A modern framework for the interpretation of $^{238}\text{U}/^{235}\text{U}$ in studies of ancient ocean redox: Earth and Planetary Science Letters, **400**, 184–194.
- Andersen, M. B., T. Elliott, H. Freymuth, K. W. W. Sims, Y. Niu, and K. A. Kelley, 2015, The terrestrial uranium isotope cycle: Nature, **517**, 356–359.
- Bezard, R., M. Fischer-Gödde, C. Hamelin, G. A. Brennecka, and T. Kleine, 2016, The effects of magmatic processes and crustal recycling on the molybdenum stable isotopic composition of Mid-Ocean Ridge Basalts: Earth and Planetary Science Letters, **453**, 171–181.
- Bourdon, B., S. J. Goldstein, D. Bourlès, M. T. Murrell, and C. H. Langmuir, 2000, Evidence from ^{10}Be and U series disequilibria on the possible contamination of mid-ocean ridge basalt glasses by sedimentary material: Geochemistry, Geophysics, Geosystems, **1**, 1029.
- Chen, S., P. Sun, Y. Niu, P. Guo, T. Elliott, and R. C. Hin, 2022, Molybdenum isotope systematics of lavas from the East Pacific Rise: Constraints on the source of enriched mid-ocean ridge basalt: Earth and Planetary Science Letters, **578**, 117283.
- Chen, S., R. C. Hin, T. John, R. Brooker, B. Bryan, Y. Niu, and T. Elliott, 2019, Molybdenum systematics of subducted crust record reactive fluid flow from underlying slab serpentine dehydration: Nature Communications, **10**, 4773.
- Cheng, H., R. Lawrence Edwards, C.-C. Shen, V. J. Polyak, Y. Asmerom, J. Woodhead, J. Hellstrom, Y. Wang, X. Kong, C. Spötl, X. Wang, and E. Calvin Alexander, 2013, Improvements in ^{230}Th dating, ^{230}Th and ^{234}U half-life values, and U–Th isotopic measurements by multi-collector inductively coupled plasma mass spectrometry: Earth and Planetary Science Letters, **371–372**, 82–91.
- Condon, D. J., N. McLean, S. R. Noble, and S. A. Bowring, 2010, Isotopic composition ($^{238}\text{U}/^{235}\text{U}$) of some commonly used uranium reference materials: Geochimica et Cosmochimica Acta, **74**, 7127–7143.
- Freymuth, H., F. Vils, M. Willbold, R. N. Taylor, and T. Elliott, 2015, Molybdenum mobility and isotopic fractionation during subduction at the Mariana arc: Earth and Planetary Science Letters, **432**, 176–186.

1942 Gale, A., C. A. Dalton, C. H. Langmuir, Y. Su, and J.-G. Schilling, 2013, The mean composition
 1943 of ocean ridge basalts: *Geochemistry, Geophysics, Geosystems*, **14**, 489–518.

1944 Gutjahr, M., M. Frank, C. H. Stirling, V. Klemm, T. van de Flierdt, and A. N. Halliday, 2007,
 1945 Reliable extraction of a deepwater trace metal isotope signal from Fe–Mn oxyhydroxide
 1946 coatings of marine sediments: *Chemical Geology*, **242**, 351–370.

1947 Hauff, F., K. Hoernle, and A. Schmidt, 2003, Sr-Nd-Pb composition of Mesozoic Pacific oceanic
 1948 crust (Site 1149 and 801, ODP Leg 185): Implications for alteration of ocean crust and the
 1949 input into the Izu-Bonin-Mariana subduction system: *Geochemistry, Geophysics,*
 1950 *Geosystems*, **4**, 8913.

1951 Hiess, J., D. J. Condon, N. McLean, and S. R. Noble, 2012, $^{238}\text{U}/^{235}\text{U}$ Systematics in Terrestrial
 1952 Uranium-Bearing Minerals: *Science*, **335**, 1610–1614.

1953 Hin, R. C., K. E. J. Hibbert, S. Chen, M. Willbold, M. B. Andersen, E. S. Kiseeva, B. J. Wood, Y.
 1954 Niu, K. W. W. Sims, and T. Elliott, 2022, The influence of crustal recycling on the
 1955 molybdenum isotope composition of the Earth’s mantle: *Earth and Planetary Science*
 1956 *Letters*, **595**, 117760.

1957 Kipp, M. A., H. Li, M. J. Ellwood, S. G. John, R. Middag, J. F. Adkins, and F. L. H. Tissot, 2022,
 1958 ^{238}U , ^{235}U and ^{234}U in seawater and deep-sea corals: A high-precision reappraisal:
 1959 *Geochimica et Cosmochimica Acta*, **336**, 231–248.

1960 Leitzke, F. P., R. O. C. Fonseca, P. Sprung, G. Mallmann, M. Lagos, L. T. Michely, and C. Münker,
 1961 2017, Redox dependent behaviour of molybdenum during magmatic processes in the
 1962 terrestrial and lunar mantle: Implications for the Mo/W of the bulk silicate Moon: *Earth*
 1963 *and Planetary Science Letters*, **474**, 503–515.

1964 Liang, Y.-H., A. N. Halliday, C. Siebert, J. G. Fitton, K. W. Burton, K.-L. Wang, and J. Harvey,
 1965 2017, Molybdenum isotope fractionation in the mantle: *Geochimica et Cosmochimica*
 1966 *Acta*, **199**, 91–111.

1967 McCoy-West, A. J., P. Chowdhury, K. W. Burton, P. Sossi, G. M. Nowell, J. G. Fitton, A. C. Kerr,
 1968 P. A. Cawood, and H. M. Williams, 2019, Extensive crustal extraction in Earth’s early
 1969 history inferred from molybdenum isotopes: *Nature Geoscience*, **12**, 946–951.

1970 Plank, T., 2014, 4.17 - The Chemical Composition of Subducting Sediments, *in* H. D. Holland and
 1971 K. K. Turekian, eds., *Treatise on Geochemistry (Second Edition)*, Elsevier, 607–629.

1972 Reinitz, I., and K. K. Turekian, 1989, $^{230}\text{Th}/^{238}\text{U}$ and $^{226}\text{Ra}/^{230}\text{Th}$ fractionation in young basaltic
1973 glasses from the East Pacific Rise: *Earth and Planetary Science Letters*, **94**, 199–207.

1974 Richter, S., A. Alonso-Munoz, R. Eykens, U. Jacobsson, H. Kuehn, A. Verbruggen, Y. Aregbe, R.
1975 Wellum, and E. Keegan, 2008, The isotopic composition of natural uranium samples -
1976 Measurements using the new $n(^{233}\text{U})/n(^{236}\text{U})$ double spike IRMM-3636: *International*
1977 *Journal of Mass Spectrometry*, **269**, 145–148.

1978 Salters, V. J. M., and A. Stracke, 2004, Composition of the depleted mantle: *Geochemistry,*
1979 *Geophysics, Geosystems*, **5**, Q05B07.

1980 Siebert, C., T. F. Nägler, F. von Blanckenburg, and J. D. Kramers, 2003, Molybdenum isotope
1981 records as a potential new proxy for paleoceanography: *Earth and Planetary Science*
1982 *Letters*, **211**, 159–171.

1983 Stracke, A., M. Bizimis, and V. J. M. Salters, 2003, Recycling oceanic crust: Quantitative
1984 constraints: *Geochemistry, Geophysics, Geosystems*, **4**, 8003.

1985 Walter, M. J., 1998, Melting of Garnet Peridotite and the Origin of Komatiite and Depleted
1986 Lithosphere: *Journal of Petrology*, **39**, 29–60.

1987 Willbold, M., K. Hibbert, Y.-J. Lai, H. Freymuth, R. C. Hin, C. Coath, F. Vils, and T. Elliott, 2016,
1988 High-Precision Mass-Dependent Molybdenum Isotope Variations in Magmatic Rocks
1989 Determined by Double-Spike MC-ICP-MS: *Geostandards and Geoanalytical Research*.

1990 Wilson, S. C., B. J. Murton, and R. N. Taylor, 2013, Mantle composition controls the development
1991 of an Oceanic Core Complex: *Geochemistry, Geophysics, Geosystems*, **14**, 979–995.
1992
1993